

Original citation:

Donchev, Evgeniy, Pang, Jing S., Gammon, P. M., Centeno, Anthony, Xie, Fang, Petrov, Peter K., Breeze, Jonathan D., Ryan, Mary P., Riley, D. Jason and Alford, Neil McN.. (2014) The rectenna device : from theory to practice (a review). MRS Energy & Sustainability - A Review Journal, 1 .

Permanent WRAP URL:

<http://wrap.warwick.ac.uk/62338>

Copyright and reuse:

The Warwick Research Archive Portal (WRAP) makes this work by researchers of the University of Warwick available open access under the following conditions. Copyright © and all moral rights to the version of the paper presented here belong to the individual author(s) and/or other copyright owners. To the extent reasonable and practicable the material made available in WRAP has been checked for eligibility before being made available.

Copies of full items can be used for personal research or study, educational, or not-for profit purposes without prior permission or charge. Provided that the authors, title and full bibliographic details are credited, a hyperlink and/or URL is given for the original metadata page and the content is not changed in any way.

Publisher's statement:

This article has been published in a revised form in <http://dx.doi.org/10.1557/mre.2014.6> . This version is free to view and download for private research and study only. Not for re-distribution, re-sale or use in derivative works.

© © Materials Research Society 2014

A note on versions:

The version presented here may differ from the published version or, version of record, if you wish to cite this item you are advised to consult the publisher's version. Please see the 'permanent WRAP url' above for details on accessing the published version and note that access may require a subscription

For more information, please contact the WRAP Team at: wrap@warwick.ac.uk

The Rectenna Device - from theory to practice (a review)

E. Donchev,^{1,*} J. S. Pang,¹ P. M. Gammon,² A. Centeno,³ F. Xie,¹
P. K. Petrov,¹ J. Breeze,¹ M. P. Ryan,¹ D. J. Riley,¹ and N. McN. Alford¹

¹*Department of Materials, Imperial College London, London, SW7 2AZ, United Kingdom*

²*School of Engineering, University of Warwick, Coventry, CV4 7AL, United Kingdom*

³*Khoza Nano-Characterization, Structural Control and Processing,
Malaysia-Japan International Institute of Technology, 54100 Kuala Lumpur, Malaysia*

(Dated: April 20, 2014)

The Rectenna (RECTifying antENNA), which was first demonstrated by William C. Brown in 1964 as a receiver for microwave power transmission, is now increasingly researched as a means of harvesting solar radiation. Tapping into the growing photovoltaic market, the attraction of the rectenna concept is the potential for devices that, in theory, are not limited in efficiency by the Shockley-Queisser limit. In this review, the history and operation of this 40-year old device concept is explored in the context of power transmission and the ever increasing interest in its potential applications at THz frequencies, through the infra-red and visible spectra. Recent modelling approaches that have predicted controversially high efficiency values at these frequencies are critically examined. It is proposed that to unlock any of the promised potential in the solar rectenna concept, there is a need for each constituent part to be improved beyond the current best performance, with the existing nanometer scale antennas, the rectification and the impedance matching solutions all falling short of the necessary efficiencies at THz frequencies. Advances in the fabrication, characterisation and understanding of the antenna and the rectifier are reviewed, and common solar rectenna design approaches are summarised. Finally, the socio-economic impact of success in this field is discussed and future work is proposed.

I. INTRODUCTION

The ever increasing global demand for clean renewable energy is a crucial topic that has major economic and societal impact for our future on this planet. The sun is a constant source of energy, thus better harvesting its radiation would solve the energy challenge and help protect the environment. Conventional solar harvesting is via the increasingly popular photovoltaic (PV) p-n junction solar cells. Although this field has seen great improvement over the last few decades since the first silicon solar cell was developed in 1941 at Bell Laboratories, its fundamental limitations discussed by Shockley and Queisser¹ in 1961 puts an upper boundary on the efficiency at around 30% for single junction solar cells¹ and 55% for multi-junction solar cells². Due to the efficiency limits of solar cells, other solar-energy converting technologies are becoming increasingly attractive. An alternative solar energy converter concept is the Rectenna (RECTifying antENNA) device, which has achieved very high efficiencies at microwave frequencies, while at THz frequencies, it has been speculated that efficiencies exceeding the Shockley-Queisser limit are achievable.

Fundamentally the Rectenna and the Solar Cell are similar as there is absorption of photons to generate a DC current. However, there is a substantial difference in their principles of operation. Solar cells are quantum devices, except for their anti-reflection coatings, and are only able to be understood and designed by the applica-

tion of quantum physics³, where light is perceived in its particle form, as photons. Hence, the efficiency is limited by the band gap energy of the active layers, where energy is lost due to low energy photons passing right through the material, and through heat loss from the high frequency photons. The rectenna device concept is different as it is based upon the wave nature of light, which is regarded as a propagating, oscillating electric and magnetic field⁴. Similar to a low pass filter in electronics, the efficient absorption of solar radiation is limited by the cut-off frequency of the device, i.e. any wavelength below this frequency can be harvested.

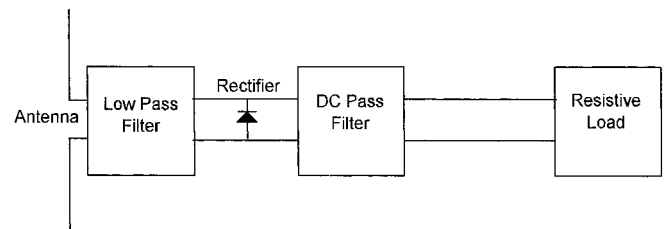


FIG. 1. Block diagram of microwave rectenna and load. (Reprinted from [3], ©2002 with permission from Elsevier)

The components of the rectenna device are shown in Figure 1. These components are commonly associated with a rectenna operating at microwave frequencies. The antenna is used to capture and convert the energy from an incoming microwave beam (or solar radiation in the case of solar rectenna) as it is an efficient transducer between free space and guided waves⁵. The electric field (E) from an incident electromagnetic wave induces an

* Corresponding author:
evgeniy.donchev07@imperial.ac.uk

alternating current (AC) in the conducting antenna. A low pass filter is used to form an impedance match between the antenna and the rectifier, and passes the signal at the tuned operating frequency whilst blocking reradiation of higher order harmonic energy produced by the rectifier^{3,6–8}. The rectifier (a diode) converts the input AC signal to a usable direct current (DC) which is transferred to the load. A DC pass filter, consisting of an inductor in series, is used to smooth the rectified signal to DC whilst providing efficient transfer to the load.

The antenna dimensions are of the same length scale as the targeted frequency⁵. Therefore, for microwave frequencies, the antenna is relatively large (cm to mm scale) compared to that required for infrared (μm scale) and optical frequencies (nm scale). Due to its smaller size, it will be difficult to incorporate the aforementioned filters into the design of a rectenna for solar energy collection. Therefore the components of the solar rectenna are reduced to just the Antenna and Rectifier (Figure 2)⁹. The removal of the low-pass filter from this design enables broadband frequency harvesting up to the cut-off frequency of the device, although it introduces the difficulty of impedance matching the antenna and rectifier, resulting in a potential drop in efficiency. Losses in transferring the rectified DC signal to the load are dependent on the diode behaviour. However, appropriate design of a DC pass filter would make its use possible in this configuration^{99,100}.

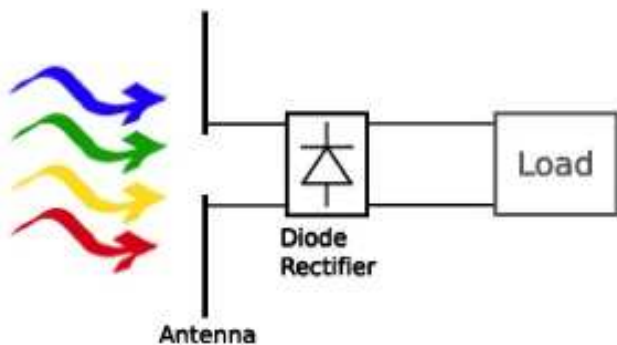


FIG. 2. Block diagram of solar rectenna and load. (Reprinted from [9], ©IOP Publishing. Reproduced by permission of IOP Publishing. All rights reserved.)

There are two families of designs for rectenna solar energy collectors. Bailey¹⁰ proposed that each antenna element is attached to its individual rectifier and the DC outputs are combined (see Figure 5). The immediate concern here is that the small voltage predicted from the antenna elements may be insufficient for rectification to occur in the attached diode element³. The only way to overcome this is to design a diode which turns on at a voltage as low as that arising from the single antenna element. The other design is by Kraus¹¹, who suggested that the electrical oscillations from many an-

tenna elements be combined in a particular phase relationship, then delivered together to the rectifier. Limitations in this design arise from the need for spatial coherence across all the antenna elements feeding the signal to the diode³. This can be minimised by appropriate design and high quality fabrication of the antenna elements.

The aim of this article is to review key research in the development of the rectenna device as an alternative or in addition to conventional solar cell technology. We aim to expand upon a few short reviews, [3–5,9,100,105], that have been published, bringing the reader up to date with a more detailed overview of the device. This article will be the first to bring together all relevant research not only on the rectenna as a whole device, but also the research on its two main components – the antenna and the rectifier. The next section will briefly describe the history of the device and how the initial application of microwave power transmission (MPT) was later modified to a solar energy harvesting alternative. Section III will analyse and discuss the many publications on experimentally and theoretically derived device efficiencies. Breakthroughs in modelling and fabricating the antenna and rectifier will be reviewed in Section IV and V respectively. Section VI will bring together all components and look at different rectenna architectures, which show potential for efficient operation at solar frequencies. We will discuss the socio-economic impact of the research in this field and proposed future work in Section VII before completing the article with a short summary in Section VIII.

II. HISTORY OF THE RECTENNA DEVICE

The rectenna concept was initially proposed for wireless power transmission by William C. Brown of the Raytheon Company in the 1960's. At the time, Brown, a pioneer of microwave power transmission, was faced with a challenge of how to efficiently receive and convert to DC power an incoming microwave beam. Wireless power transmission was not a new concept as it had begun with the ideas and demonstrations by Tesla in 1899 using radio waves¹². Tesla managed to demonstrate this concept although never found an applicable route into its commercialisation.

In 1959 the Raytheon Company proposed the Raytheon Airborne Microwave Platform (RAMP) concept to the US Department of Defence as a solution to communications and surveillance problems¹³. This proposed platform was to be flown at high altitude (50,000 ft) in the form of a helicopter, powered by microwave transmission. The US Department of Defence did not fund the project however the Raytheon Company pursued their interest by researching the required technological developments for its realization. One missing technology was a suitable microwave rectifier¹⁴, capable of converting the microwave signal directly into the DC current necessary to power the platform's motors and stay airborne. Their initial design used a

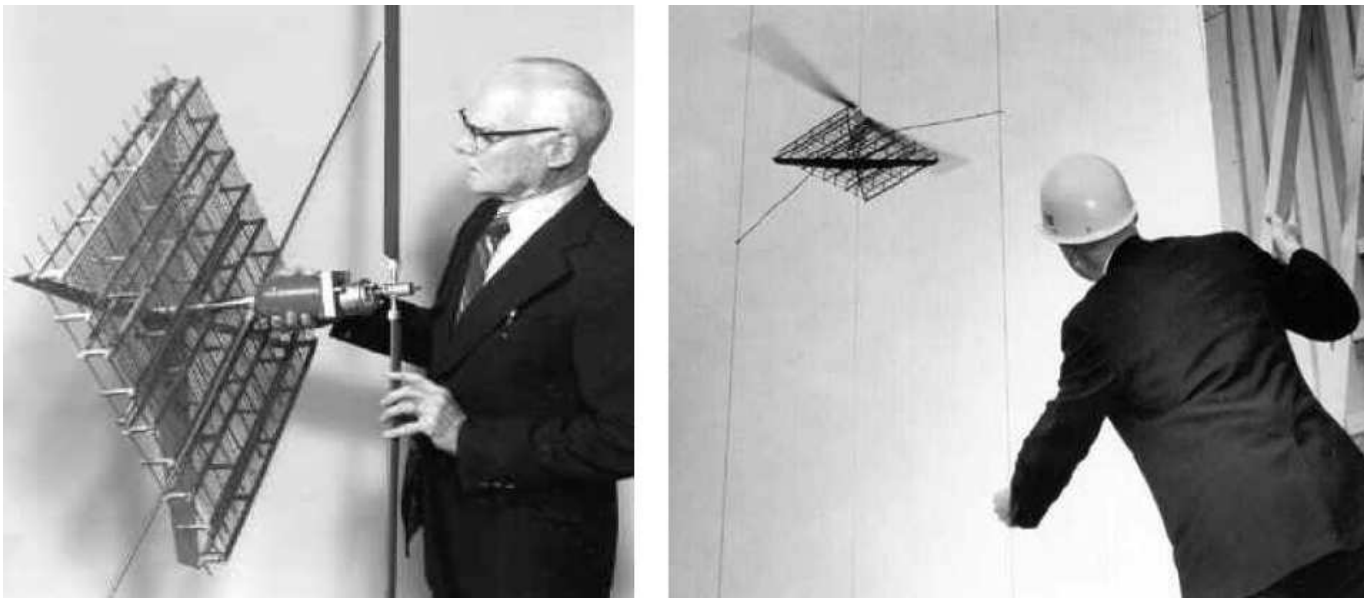


FIG. 3. Left: W.C. Brown holding the rectenna helicopter platform. Right: In flight demonstration of the rectenna helicopter on October 1964. (Reprinted from [17])

horn-illuminated ellipsoidal reflector that focused the microwave beam into a trapezoidal horn at a 20 ft distance where the microwaves were converted to DC power by the rectifier¹³. Using this first design, Brown constructed and flew thirty feet above his lawn, a small tethered helicopter that he had built with his son in his own workshop¹³. Although this concept worked, Brown was aware of the flaws in his system and continued to work on other possibilities.

In 1963, Brown met with his colleague and friend Roscoe George, a professor at Purdue University who had been working on a microwave point-contact semiconductor diode¹⁵. Following discussions regarding his challenge, a device which is now known as “Rectenna” was conceived. The proposed solution was patented in 1969 and consisted of taking individual full-wave rectifiers out of the waveguide, attaching them to half-wave dipoles, and placing a reflecting plate behind the structure¹⁶. The first microwave rectenna was built by R.H. George at Purdue University but conceived at Raytheon Company in 1963, shown in Figure 4. Later in 1964, Brown built a helicopter which had an array of 28 such Rectennas. The helicopter was demonstrated in flight 60 ft above a transmitting microwave beam on the CBS Walter Cronkite News in October 1964. Figure 3 shows some impressive images of this historic event. The interested reader is referred to Brown’s recollection on “The History of Power Transmission by Radio Waves” in [13], where all the interesting details and facts about the invention of this device can be found.

Following this invention, microwave power transmission became very popular and many potential applications were researched. An interesting one is the solar

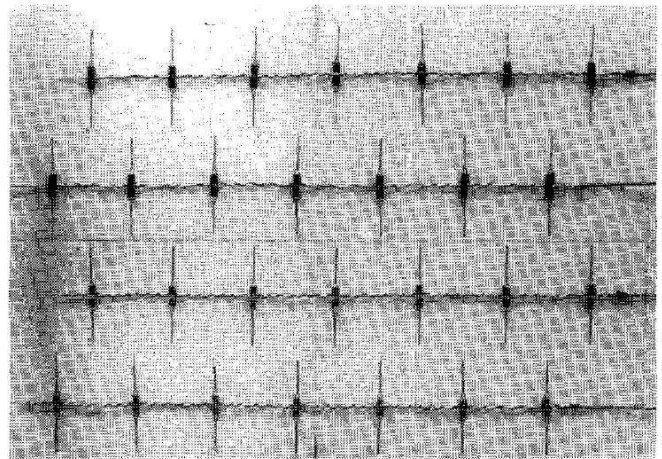


FIG. 4. The first rectenna. Conceived at Raytheon Company in 1963, built and tested by R.H. George at Purdue University. It was composed of 28 half-wave dipoles, each terminated in a bridge rectifier made from four 1N82G point-contact, semiconductor diodes for operation at 2.45 GHz. A power output of 7W was produced at 40% efficiency. (Reprinted from [13], ©1984 IEEE. Reprinted, with permission, from IEEE)

power satellite (SPS), proposed by P. E. Glaser¹⁸ in 1968. The concept of the SPS represents a 5 GW power station on the geostationary orbit, which collects electrical power by means of solar cells and transmits microwaves of the 2.45 GHz band to a rectenna array site on the ground. The SPS project was researched by Brown and Glaser^{19–22} which earned Glaser a patent in 1973²³ and

a collaborative three year project together with Brown in 1977 called the “DOE/NASA Satellite Power System Concept Development and Evaluation Program”. The work ended in 1980 with much success in developing new ideas in the design of transmission technology and rectenna arrays however did not attract further funding. Although this was the end of the SPS initiative in the US, some experimental studies of the concept were seen in the 1990s in Yamasaki, Japan^{24,25}. The interested reader is referred to Glaser’s overview of SPS progress in [26].

The developments from the SPS project yielded other applications involving microwave transmission and rectenna, such as intersatellite power transmission²⁷, including utility power satellites²⁸, mechanical actuators for space-based telescopes²⁹, small dc motor driving³⁰, short range power transfer as for example between two parts of a satellite, RF identification tags (RFID) and biomedical implants³¹. These applications all include single band rectenna operation. Hagerty *et al*³¹ have shown a broadband rectenna array for microwave operation to be used in low-power indoor sensor networks and RF energy recycling. Recent publications have shown a compact printed rectenna that can be used to supply DC power to electrical devices supporting data communication systems³².

The idea of exploiting the wave nature of light, or solar radiation, and converting its energy into usable direct current by the use of antennas, originated as part of a NASA summer project in the late 1960s undertaken by J.C. Fletcher of NASA and R.L. Bailey of the University of Florida⁴. The first official report of this concept was published by Bailey in 1972¹⁰. In this paper, he named his device the “*Electromagnetic Wave Energy Converter (EWEC)*” and suggested an artificial pyramid or cone structure as antennas, analogous to those found in nature and similar to dielectric rod antennas. The paper described pairs of pyramids as modified dipole antennas, each pair electrically connected to a half-wave rectifying diode, filter and load. This invention is fundamentally very similar to the initial microwave rectenna proposed by Brown, but it is modified so that the antenna and rectifier operate at much high frequencies to harvest solar energy. The device called by Bailey EWEC is now referred to as a Solar Rectenna.

Bailey’s first publication on the subject in 1972 served as a proof of concept as he showed the broadband characteristics of his pyramidal antennas by tests at 100-1000 MHz. Following this, in 1973, Fletcher and Bailey published a patent³³ on the EWEC concept. Later in 1975, in their final report, Bailey *et al*³⁴ presented their theoretical work highlighting the importance of future research into optimised antenna design and fabrication, while not forgetting that rectification of the signals was an equally critical issue and a significant challenge⁴. These two components of the rectenna solar energy harvester are now of equal research interest (see Sections IV & V).

Later, alternative rectenna structures were proposed

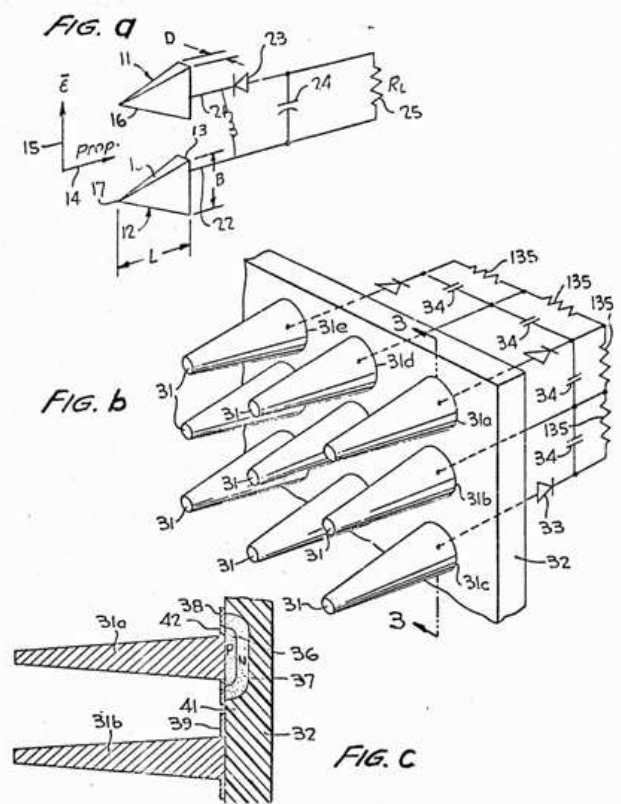


FIG. 5. The EWEC concept by Fletcher & Bailey. Each broadband conical antenna is connected to a rectifying diode, filters and load. (Reprinted from [33])

and patented by Marks^{35–38}, who was inspired by the earlier half-wave rectifier EWEC concept. His first patent in 1984 was a device with arrays of submicron crossed dipoles on an insulating sheet with fast full-wave rectifiers³⁵. Later in 1988, Marks was first to patent antenna-like cylinders attached to asymmetrical metal-insulator-metal (MIM) diodes for rectification³⁷. MIM diodes are one of the most promising rectifiers for use in Infrared and Optical Rectennas and will be later discussed (Section V.B).

The first reported experimental evidence of a fabricated resonant nanostructure absorbing and rectifying at visible light frequency was published by Lin *et al*³⁹ in 1996. They recorded a short circuit current using a parallel dipole sub-nanostructures connected to a p-n junction for the rectification of the absorbed signal. Credit must be given also to Gustafson & Billman⁴⁰ who first suggested harvesting visible radiation in 1974. Their work formed the basis of using optical diodes like the MIM diode.

Figure 6 outlines a brief timeline of the key events that have lead to the current research activity in solar rectenna. Further reading is suggested in [3,4] for a more detailed reference and explanation of the major historic breakthroughs in the field of solar harvesting by rectenna.

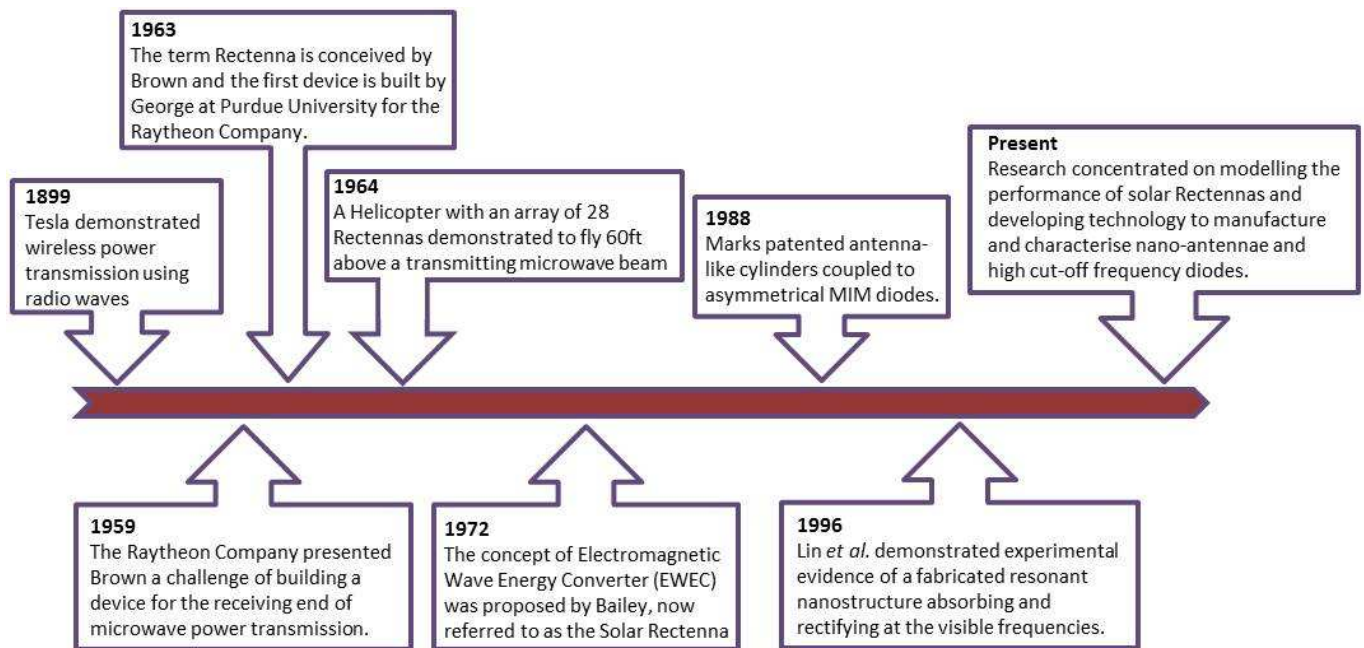


FIG. 6. Brief timeline of the rectenna device - from concept for microwave power transmission to research focused on solar harvesting

In the following sections, we mainly focus on the key research in harvesting optical and infrared frequencies using the rectenna concept.

III. EFFICIENCY LIMITS

The first rectenna device (Figure 4), which was built in 1963, provided a 7 W power output with 40% efficiency¹³ designed to work at 2.45 GHz. This was the most commonly targeted transmitting frequency for MPT because of its low attenuation through the atmosphere even in severe weather and being at the centre of the industrial, scientific, and medical (ISM) band meant that it was the most advanced and efficient transmitting technology.

This rectenna used half-wave dipole antennas to receive the signal and point-contact semiconductor diodes for rectification. In later device attempts, the half-wave dipole antenna remained the preferred technology, but an increase in efficiency was mainly achieved by improving the rectifier performance, incorporating Schottky Barrier Diodes (SBD). From the early 1960's until the early 1980's there has been a steady increase in the experimentally demonstrated efficiency of the rectenna at 2.45 GHz (Figure 7a). Although Nahas⁷ first developed a model (using a distributed transmission-line technique including skin-effect losses) to simulate the top performance of a rectenna utilising a dipole antenna and a conventional SBD, his prediction of an 80% upper boundary (most of the losses came from the diode rectifier) was later im-

proved when Brown⁸² experimentally demonstrated what is to date, the highest ever recorded efficiency at the 2.45 GHz band of 92%. This was made possible by using the then well established Pt/GaAs Schottky diode and supported Brown's predictions that 100% efficiency is possible for this device^{44,82}.

In another attempt to model the efficiency, Gutman & Borrego⁵¹ predicted an upper boundary of 85% incorporating numerous rectifier outputs interconnected to a common DC load. They used a closed-form analytical circuit model and a computer-simulation model in an attempt to show that a higher output power can be achieved having an array of these components as opposed to a single rectenna element.

It is important to state that the conversion efficiencies (η) considered here are simply defined as the ratio of the output power (P_{out}) over the power incident on the antenna (P_{in}),

$$\eta(\%) = \frac{P_{out}}{P_{in}} \times 100 \quad (1)$$

One of the most successful demonstrations of MPT was in 1975 by Dickinson and Brown⁴² who used an array of 5000 rectennas to receive a transmitted signal over a distance of one mile with 82% efficiency at 2.388 GHz^{42,43}. The rectenna architecture again contained half-wave dipole antennas. In the last two decades many other antenna architectures have been proposed in search of enhanced performance and economical alternative. These include the microstrip patch^{44,46}, circular polarised^{53,56-58}, compact slot ring⁵⁵

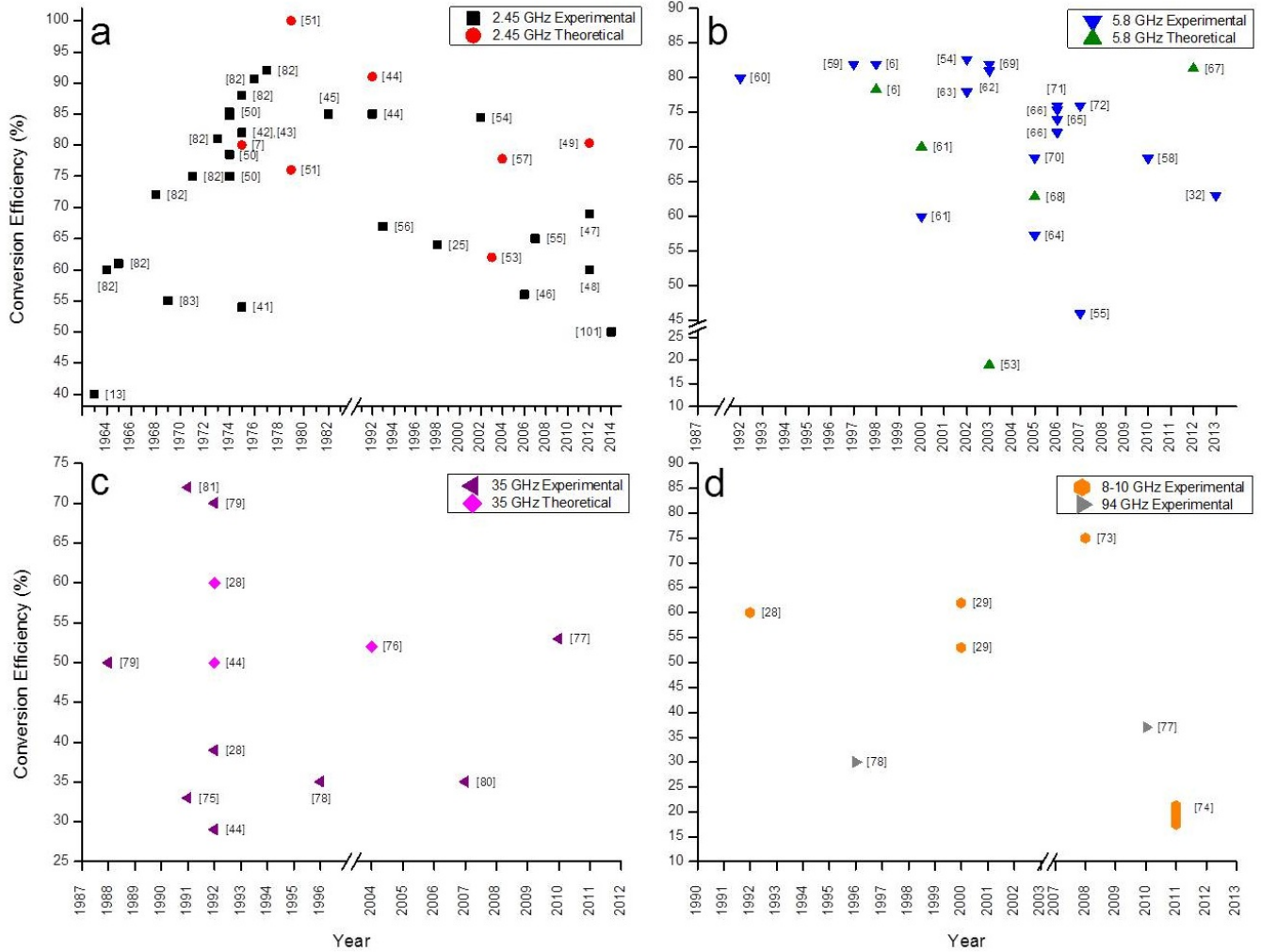


FIG. 7. Reported conversion efficiency (as defined by their authors) evolution over the years of a rectenna device for Microwave Power Transmission. Data points are split into Experimental and Theoretically derived values of efficiency. a) 2.45 GHz, b) 5.8 GHz, c) 35 GHz and d) 8-10 GHz and 94 GHz. [**] indicates the reference corresponding to the data point. Data collected from [3,5–7,10,11,13,25,28,29,32,41–51,53–82,101]

and shorted annular ring-slot^{47,53} antennas with all attempts returning efficiencies between 55 and 85% (see Figure 7a). The higher efficiencies reported all used GaAs Schottky diodes as opposed to conventional Si Schottky diodes, showing the importance of diode behaviour on device performance.

In the 1990's a renewed interest in the solar power satellite (SPS) concept^{18–26} started a new focus of research into high efficiency rectennas and rectenna arrays operating at higher frequency than the mid-ISM band (2.45 GHz)⁴¹. With higher operating frequency, the device dimensions can be reduced conveniently from the point of SPS construction feasibility⁴¹. Also small size design can be appropriately implemented in a range of other applications such as a supply source in RFID^{31,55,58,64,68,77}, wireless sensors^{31,47,58,77} and data communication systems^{32,61,64,65,67,77}. Rectennas oper-

ating in the C-band (≈ 5.8 GHz – Figure 7b), X-band (8-10 GHz Figure 7d), K α -band (35 GHz Figure 7c) and W-band (94 GHz Figure 7d) have appeared after the 1990s, some even operating in two bands (2.45 & 5.8 GHz^{53–55} and 35 & 94 GHz⁷⁷). However, the efficiency is different in the two frequency bands with the higher frequency operation yielding lower efficiency due to losses in transferring the AC signal generated from the antenna to the rectifier circuit. The only dual frequency rectenna with high efficiency in both bands is reported by Suh & Chang⁵⁴ with an excess of 82% efficiency at both 2.45 and 5.8 GHz employing a CPS dipole antenna and GaAs SBD.

At 5.8 GHz, efficiency values in the range of 60-85% have been both predicted^{6,61,67,68} and demonstrated^{6,32,54,59–63,65,66,69–72} with different approaches returning equally successful devices through

the years (Figure 7b). The few experimentally reported rectennas at 8-10 GHz have seen slight improvement in efficiency when a circular or dual polarised printed patch antenna has been coupled to the GaAs^{28,29} or Si⁷³ Schottky diode, however with a planar slot antenna⁷⁴ the efficiency is only 21.2% (Figure 7d). At 35 GHz (see Figure 7c) theoretical predictions are higher than their corresponding experimental results^{28,44}, although with a similar antenna and diode design, high experimental efficiency of 70% has been reported elsewhere [79,81]. Analysis of the different efficiencies achieved with similar rectenna technologies highlight the importance in the circuit and device design for rectennas used in microwave power transmission. Furthermore, load impedance and the power of the incoming beam also affect the overall efficiency of the device.

It can be noticed from Figure 7 that for a given frequency some models predict a lower efficiency than that which had already been experimentally achieved. The reason is that over the years, new antenna and rectifier technologies, and alternative, more compact circuit designs were emerging, which could not improve or even match the record efficiency achieved with the half-wave dipole antenna and Pt/GaAs SBD. Furthermore, scaling down the components and aiming towards higher frequency operation at lower cost, introduced difficulties for appropriate circuit design and the efficiency suffered a continuous drop. Overall, considering the evolution of reported efficiencies over the years (Figure 7) for MPT rectennas, it can be concluded that with appropriate antenna design, good matching to a suitable well-functioning diode rectifier connected to a DC load, experimental evidence of efficiencies over the 70% mark can be obtained for frequencies up to 35 GHz (see also Figure 8).

The high efficiencies achieved at the low GHz frequencies are due to the ease of fabricating the devices and designing appropriate filters (low pass and DC pass – see Figure 1). To be able to receive a signal, the antenna has to be of the same length scale as the wavelength of the incoming wave, which at the low GHz frequencies ranges from a few mm to 10's of cm. At infrared and optical frequencies, wavelengths are from μm to nm, which subsequently indicates the necessity of building the antenna and rectifier in this length scale range. At this scale, a direct impedance match of the antenna to rectifier has to be achieved (Figure 2) instead of using a low-pass filter, which cannot be designed at such small dimensions. This is what Bailey's proposed electromagnetic wave energy converter¹⁰ implies – a scaled down version of Brown's rectenna consisting of a μm length antenna connected directly to the diode rectifier transferring the output to the load through a DC pass filter of some sort. Bailey predicted an efficiency in excess of 50% for his EWEC device at microwave frequencies, although not backed by any modelling or experimental evidence of a whole device. The only evidence he gives is the ability of an EWEC prototype to absorb electromagnetic plane

polarized waves at 475 MHz. His vision was to study the concept at microwaves and later scaling it to light frequencies where he speculates potential for unity efficiency. A MPT rectenna device without a low-pass filter is possible and was demonstrated in 2012 at 2.45 GHz⁴⁷. The proposed printed shorted annular ring-slot rectenna is designed to match the impedance of the SBD rectifier at 2.45 GHz. The diode however will produce second and third order harmonics which will re-radiate at 4.9 and 7.35 GHz but these will be blocked because the antenna is designed to mismatch its impedance at the higher order harmonics thus preventing re-radiation⁴⁷. This device architecture removes the need for a low-pass filter design and achieves 69% efficiency.

Apart from Brown^{45,82} (for microwave) and Bailey¹⁰ (for solar) several other authors (Kraus¹¹, Balanis⁸⁶, and Andersen & Frandsen¹⁰⁷) have speculated about the possibility of 100% conversion efficiency coming from highly absorptive no-loss antennas and ideal matching, transferring and rectification of the absorbed input signal to the load. This antenna efficiency is assuming uniform distribution of energy across the antenna, a single frequency and a coherent source. The high efficiency values for MPT are achieved not only with appropriate antenna design, matching circuit and rectifier performance, but also with efficient delivery of a good signal, because the artificially created microwave signal is single band, polarised and coherent. This makes the antenna engineering easier. Simply reducing the size of the components to operate at solar frequencies does not necessary mean that the efficiency will remain as high as that observed for MPT Rectennas. Unlike monochromatic microwave radiation, sunlight is unpolarised, incoherent and distributed over a wide band of wavelengths⁹⁶. This creates further challenges in antenna engineering and lead to disputes on how to model the device performance. Furthermore, the diode has to be optimised to rectify the signal at the higher frequencies and both antenna and diode have to be well matched to maximise power transfer.

Provisional tests at 10 GHz with a dipole antenna and a Schottky diode were demonstrated by ITN⁵ estimating efficiencies of over 50% however this frequency is too low for solar energy harvesting. ITN state that the lower frequency rectenna is scalable to the higher THz frequencies required for solar harvesting with their models predicting up to 85%⁵ efficiency. According to microwave antenna theory, the antenna length scales linearly with the incident frequency which means that in theory the antenna can be scaled to resonate at IR and optical frequencies⁵. This is not entirely the case because at IR and optical frequencies the conduction is not Ohmic and the scaling laws are rather an estimation than an accurate representation of the real-life situation as the majority of the energy in the surface modes is carried in the dielectric above the antenna. This symbolises the importance of impedance losses. The antenna has to be designed to resonate against a complex waveform

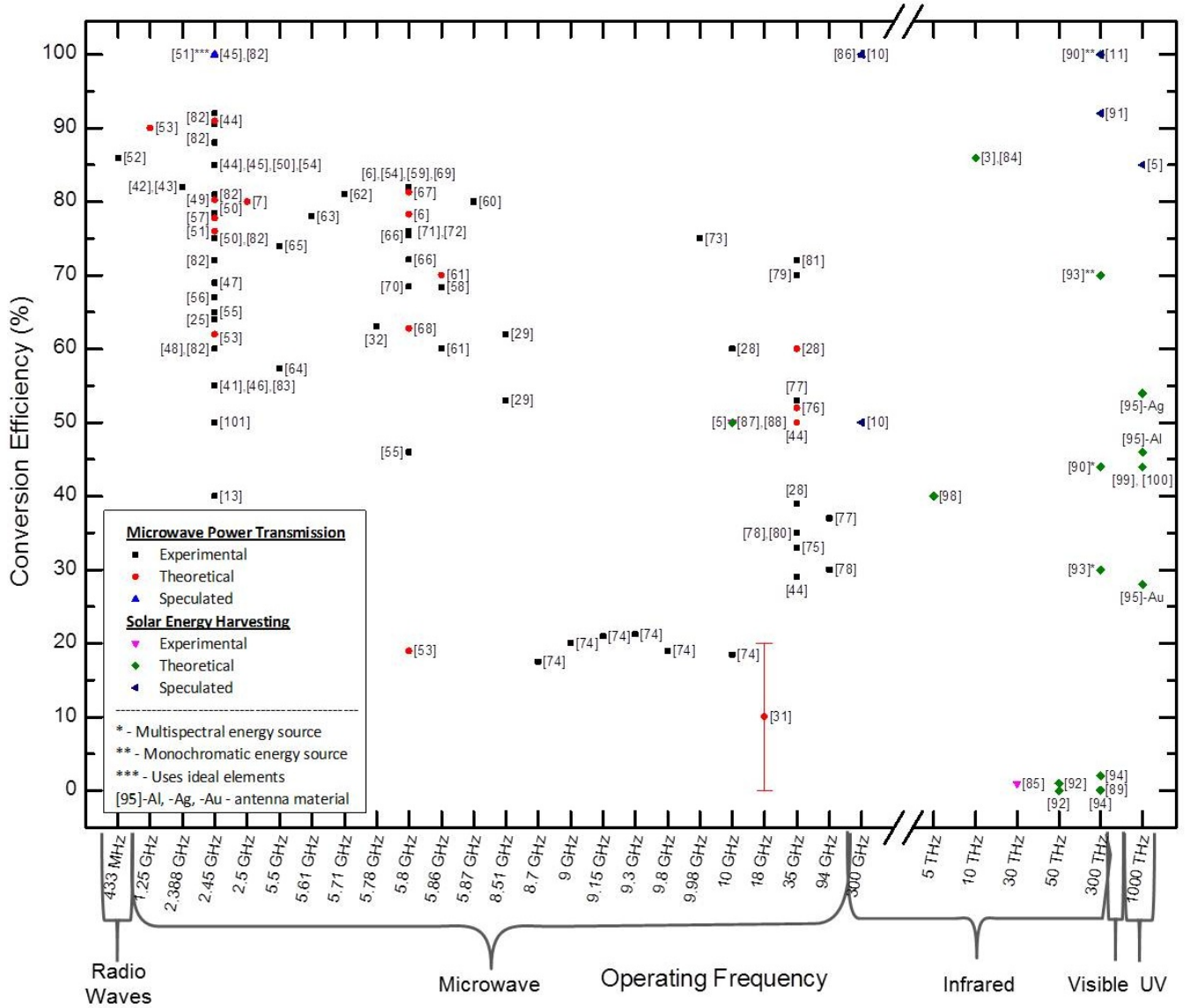


FIG. 8. Reported conversion efficiencies (as defined by their authors) at their maximum operating frequency of a rectenna device. Data points are grouped by the two applications of the rectenna - either Microwave Power Transmission or Solar Energy Harvesting, each displaying experimental, theoretical or speculated efficiency values. [**] indicates the reference corresponding to the data point. Data collected from [3,5-8,10,11,13,25,28,29,31,32,41-101]

and absorb broadband solar radiation which ranges from about 150 to 1000 THz, 85% of which corresponds to a wavelength of between $0.4\mu\text{m}$ to $1.6\mu\text{m}$ ⁵. To reach the targeted frequencies in the high THz region, SBD rectifiers would not meet the criteria as the best cut-off frequencies are only up to a few terahertz¹⁰³. MIM diodes are used for their potential to work in the higher THz region. The first practical demonstration was done by NIST⁸⁵ who used atomic layer deposition grown Cr/CrO_x/Au diodes coupled to a dipole antenna and measured its efficiency at 30 THz (achieved using a CO₂ laser) to be below 1%. This attempt was carried

out on an un-optimised antenna structure with a poor MIM diode. Following this, numerous theoretical models have been proposed, predicting the overall conversion efficiency of the solar rectenna (see Figure 8). For MPT rectennas, most theoretical and experimental efficiency results tend to be of the same order, whereas it can be seen that for Solar rectennas different attempts on modelling the performance predict a spread of efficiencies. Some approaches are close to the Landsberg limit of 93.3%¹⁰² whilst others predict discouraging figures below 1% (Figure 8).

Conversion efficiencies from 0.001% to 2% have been

theoretically derived^{89,92,94} employing various assumptions and a variation of modelling approaches (Figure 8). Mashaal & Gordon⁸⁹ analysed the efficiency in terms of losses by the state-of-art rectenna designs which adopt single polarization antennas able to convert only half of the random-polarization input power from solar radiation and a half-wave rectifier blocking the negative voltages of the input signal. Their assumptions were based on ideal matching between antenna and rectifier, zero turn-on voltage, limitless switching speeds and non-filtered signal output from the antenna prior to entering the rectifier which yielded an overall conversion efficiency of 0.0795% and four times as high if a full-wave rectifier is employed. It is a common misperception that with rectennas, the diode forms a half-wave rectifier, which would hold true for a single diode in a series configuration. However, common rectenna design incorporates a diode connected in parallel, which forms a clamp circuit capable of rectifying the full wave^{99,100}. Therefore, estimating rectenna conversion efficiency should not be discouraged by assuming a half-wave rectification mechanism. Instead, efforts should be concentrated in understanding the effect of impedance mismatch. Briones *et al.*⁹² based their model on the assumption that the collection of EM radiation by the antenna is done efficiently, which resulted in 0.001% efficiency of the system due to impedance mismatch losses between antenna and rectifier and inefficient rectification of the signal. By assuming efficient rectifier performance, the potential efficiency rises to approximately 1%.

An equally important criterion for efficient device operation is antenna material selection. Vandenbosch & Ma divided the analysis on the efficiency of nano-rectennas into two parts – 1) the efficiency by which the light is captured by the antenna and brought to its terminals⁹⁷ and 2) the efficiency by which the captured light is transformed to low frequency power by the diode^{95,96}. Considering first the antenna efficiency, they studied various antenna materials in the form of 250 nm dipoles placed on a substrate⁹⁷. Their calculations predicted antenna efficiency of 61.6% for Ag, 50.3% for Al, 34.3% for Au, 29.5% for Cu and 9.4% for Cr. In a later paper, [95], they looked at the diode efficiency and more specifically, investigated the power loss due to impedance matching whilst assuming efficient signal rectification. This analysis was only done on the highest performing materials – Ag, Al and Au. Their work was a continuation of a previous work by Sarehraz *et al.*⁹⁶, however their analysis covered 75% of the power radiated by the sun (up to 1000 THz) whereas Sarehraz *et al.* only based their analysis on 15% of the spectrum. Although Al gave the best matching efficiency of 97%, the best overall conversion efficiency of the rectenna considering both constituent parts is with Ag which gives 54% whereas Al would have 46% and Au just 28%⁹⁵ (Figure 8). So far the analysed publications all share a united opinion that a suitable rectifier is needed in order for the above mentioned efficiency estimates

to be achieved or improved. For impedance matching, Ma & Vandenbosch⁹⁵ suggest that the impedance of the rectifier must be of the order of 100Ω both for the real and imaginary part and favour aluminium as being a suitable material for this application.

A governing factor in rectifier performance is its RC time constant which defines the cut-off frequency, f_c . This is the upper limit at which the rectification process is efficient. Above the cut-off frequency, rectification is still possible however the strength of the rectified signal at the output of the MIM will drop by a factor of approximately $(f_c)^2$, thus the higher the frequency above f_c the lower the rectification efficiency⁹⁶. The cut-off frequency is estimated by the following expression proposed by Sanchez *et al.*¹⁰⁴,

$$f_c = \frac{1}{2\pi RC} \quad (2)$$

where R is the series resistance and C is the capacitance. The cut-off frequency of the whole rectenna device can be evaluated by the following relation, which considers the antenna impedance (R_A) and diode resistance (R_D)⁹²,

$$f_c = \frac{R_A + R_D}{2\pi R_A R_D C_D} \quad (3)$$

To achieve a high cut-off frequency, the RC constant must be small, which can be obtained with a small junction area¹⁰⁴, and appropriate material selection and fabrication. MIM rectifiers, although the most promising rectifier technology, have not been demonstrated at high THz frequencies with the best MIM diodes operating only up to 150 THz ($\lambda = 2 \mu\text{m}$)⁵ (more detail in Section V). Improving MIM fabrication technology and material system design would potentially yield the solution to the rectenna efficiency.

So far, the reviewed efficiencies were all based on classical approaches, not concerning thermodynamic limits to solar energy conversion. In terms of equilibrium, an antenna receiving power from any source and transferring it to the load must transmit the same amount of power back to the source³. If the power is extracted from the load, the reduction in its temperature will introduce a different approach to analysing the energy balance between the incoming, extracted and reradiated powers. In this case, Corkish *et al.*³ state that the system would have the same conversion efficiency limit as the one expected for a solar thermal collector. Assuming the Sun to be a 6000 K black body and the surroundings to be at 300 K, this limit is 85.4% for mono-spectral energy conversion and 86.8% for multi-spectral. Further analysis suggests that the Landsberg¹⁰² limit of 93.3% can be reached due to certain benefits that the rectifying diodes have in rectennas (see [3] for more details), however this is hard to justify due to the generation of thermal noise by the rectifiers. Diodes cannot rectify their own thermal noise as it violates the second law of thermodynamics (known as Brillouin's paradox¹⁰⁶).

Lerner *et al.*⁹³ developed a thermodynamic expression

for the open circuit voltage and conversion efficiency of a rectenna with the rectification process based on the geometric property of the antenna tip which provides a connection to the circuit and creates a tunnel junction. They envisioned the possibility of using advanced nanofabrication techniques and a selective atomic layer deposition process to manufacture nanometer junctions which would potentially allow for rectification of blue light frequencies⁹³. In modelling the circuit of the rectenna, it can either be considered as a constant voltage source with an emf independent of the load resistance or as a constant current source whose emf depends on the load resistance. As suggested by Lerner *et al.*⁹³, the rectenna device is more appropriately modelled as a constant current source in which case efficiencies are predicted in excess of 70% for a monochromatic light source and an optimised device. Should the device be tuned for multiphoton absorption, the efficiencies are expected to be further enhanced⁹³. The question remains as to whether a suitable technology is yet available to make such structures.

Another analysis on the broadband blackbody radiation response of optical rectennas was done by Joshi & Moddel⁹⁰ by using the theory of photon assisted tunnelling. By assuming negligible reverse current of the diode, zero dark current turn-on voltage and perfect matching to the antenna, the device power conversion efficiency at monochromatic light can approach 100%, whereas for multispectral light the value is approaching a maximum at 44% at an operating voltage of 1.1 V. It should be noted that these authors also suggest that spectral splitting is likely to improve the efficiency. This can be achieved by setting the operating voltage for each rectenna to rectify the desired spectral range, thus implying that the operating voltage for the diodes in rectennas has a similar role to the band-gap as a limiting factor in photovoltaic devices⁹⁰.

With its proven success to receive and rectify monochromatic microwave beams with high efficiency, there is a growing interest in establishing the true potential of the rectennas' ability to convert solar radiation. As seen in Figure 8, there are many theoretical approaches predicting this, however there is no one universal theory that clearly states whether the solar rectenna can compete with, let alone surpass common photovoltaic cells. There is however, the common opinion between scientists worldwide that the technology is not mature enough to fabricate a device of comparable efficiency. Advances in antenna engineering suggest that it is now possible to manufacture nano sized antennas which can absorb solar radiation from the infrared to the visible frequencies (Section IV). Work on the rectifier component has seen great progress over the years with many attempts showing great potential for use in rectenna devices (Section V).

IV. ANTENNA

Antennas are used either as transmitters, to create electromagnetic (EM) waves that have a well-defined radiation pattern, or as receivers of EM waves from a remote source⁸⁶. The purpose is usually to send or extract information that is encoded into the EM wave. Antennas are now essential in many aspects of modern day living, the mobile phone being the most common example. They normally operate at a resonance. Typically this is a half wavelength dipole antenna. The resonant wavelength of the antenna will be at the wavelength of the incoming propagating signal and energy is then transferred between them. For this reason, the antennas are usually fabricated in the dimensions of the wavelength of the incident wave. A higher frequency thus requires a smaller antenna. However, an antenna designed to be resonant at a very specific frequency by only considering a linear dimension does not guarantee efficient energy absorption. Other factors such as impedance mismatch in the circuits, bandwidth, direction and polarisation of incidence radiation needs to be considered. The aim of this section is to introduce some different designs of antennas for microwave and optical frequencies.

Most antennas at microwave frequencies are designed to work within a specific frequency band reserved for industrial, scientific and medical (ISM) frequency use. For example, one of the most popular frequency bands is 2.4 – 2.5 GHz, which devices such as wireless networks, near-field communications, and Bluetooth use. Therefore these antennas only require millimeter dimension. A dipole antenna is one of the simplest designs. It consists of two identical metal elements in mirror symmetry. The most common form is two metal rods aligned on the same axis. The length of the metal rods is half the size of the resonance wavelength. Higher-order resonance modes also occur in the same antenna but at reduced efficiency due to attenuation of the induced current in the antenna. Nevertheless, the accepted frequency bandwidth is very narrow. A slight variation of the incoming frequency gives rise to parasitic capacitance and inductance resulting in inefficient energy absorption. Therefore, a precise fabrication of the antenna is necessary. This increases the difficulty in manufacturing good devices, especially when the frequency of interest is higher.

One method to circumvent the narrowband absorption problem, which dipole antennas encounter is to extend the arms width above the standard limit (i.e. 5% longer than the wavelength)¹⁰⁸, allowing a bigger window of frequency acceptance. This type of antenna is referred to as the bow-tie antenna (Figure 9). The length of each arm is half the size of the radiation of interest. However, the correct length of the antenna alone does not guarantee high efficiency absorption since the incoming wave has various angles of incidence and polarisation¹⁰⁹. To overcome this problem, a variety of designs have been investigated, such as spiral^{108,110} (Figure 9), log-periodic^{108,110}, microstrip slot¹¹¹, and retrodirective rectenna array¹¹².

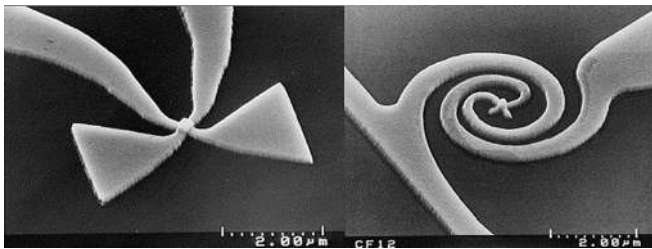


FIG. 9. SEM images of (left) bow-tie antenna with integrated Ni-NiO-Ni diode and (right) spiral antenna. (Reprinted from [108], ©1998 with permission from Elsevier)

As previously discussed in Section III, at microwave frequencies, antennas can be designed to be very efficient. Achieving such high efficiencies at the higher frequencies is more challenging with scaling down antennas. The solar spectrum emits energy across a broad band, which implies that the antenna must absorb a large bandwidth of solar frequency, otherwise most energy will be lost. For an antenna to operate efficiently at optical frequencies it is necessary to adjust both the inductance (L) and capacitance (C) to bring the device resonance to the required short wavelength. This would require both L and C to be very small¹¹³. To achieve this, the dimensions of the antenna must be reduced to the scale of the optical wavelength, i.e. nanometer. Scaling down the conventional antenna design to nanometer is of interest, as it can be determined whether classical antenna theory remains valid. For example, electron beam lithography has been used to fabricate a dipole antenna with a 3.5 nm NiO layer, sputtered between the two Ni antenna arms¹⁰⁹. The dipole antenna had a total length of 6.7 μm and was designed for 10 μm wavelength (30 THz). Another example is of a gold dipole antenna fabricated by using focus ion beam (FIB) milling¹¹⁴.

These attempts have proven it impossible to scale classical antenna designs to the optical frequency regime. At radio frequency the metals used for the construction of antennas can be considered almost lossless. This allows a large variation of radio frequency antennas to be designed by considering the metal to be a perfect conductor. However, the losses become increasingly significant as the frequency rises. This is due to the finite effective mass of electrons causing the electrons to react with increasing phase lag to an oscillating EM field¹¹⁵. As soon as the phase lag approaches 90° the amplitude of the charge oscillation goes through a maximum and is only limited by the Ohmic and radiation damping of the system¹¹⁶. In metallic nanoparticles this resonance corresponds to the localized surface plasmon resonance (LSPR). For gold, silver, aluminium and copper the LSPR is in, or very close to the visible light part of the spectrum. The LSPR can be exploited to overcome some of the drawbacks of antennas at optical frequency, in particular the high Ohmic losses compared to microwave frequencies.

A. Properties of Metals at Optical Frequencies

The optical response of metals can be described by a complex frequency-dependent dielectric function,

$$\epsilon(\omega) = \epsilon_1(\omega) + i\epsilon_2(\omega) \quad (4)$$

The electric field is related to the induced polarization density as¹¹⁷,

$$P(\omega) = \epsilon_0[\epsilon(\omega) - 1]E(\omega) \quad (5)$$

For optical antennas, Ohmic losses in the metal should be minimized. The Ohmic absorption is proportional to the conductivity of the material, $\sigma(\omega)$, which is related to the dielectric function by.

$$\epsilon_2 = \sigma(\omega)/\epsilon_0\omega \quad (6)$$

Ohmic losses take place in close proximity to the surface of the metal, within the so-called penetration depth¹¹⁸, which for metals at visible wavelengths are of the order of several nanometers (approximately 13 nm and 31 nm for aluminium and gold at 620 nm wavelength, respectively)¹¹⁹. The dielectric properties of a metal can cause a LSPR in the visible spectrum, which is connected to large local fields, and enhanced scattering and absorption.

At optical frequencies the metal conduction electrons may be treated as an ideal electron gas. The collective behaviour of this free electron gas can be expressed using the Drude-Sommerfeld model¹¹⁸,

$$\epsilon(\omega) = \epsilon_\infty - \frac{\omega_p^2}{\omega^2 + i\gamma\omega} \quad (7)$$

where ω_p is the volume plasma frequency and γ is a damping constant¹¹⁸. (For Au at optical frequencies $\omega_p = 13.8 \times 10^{15} \text{s}^{-1}$ and $\gamma = 1.07 \times 10^{14} \text{s}^{-1}$)¹¹⁶

The Drude-Sommerfeld model does not account for interband transitions due to photons with high-enough energy promoting electrons from lower lying valence bands to higher energy conduction bands¹²⁰. This can be described using a Lorentz model of the dielectric function, which is described by a collection of damped harmonic oscillators with well-defined resonance frequencies, ω_0 ,

$$\epsilon(\omega) = \epsilon_\infty + \sum_{i=1}^n \frac{\alpha_i \omega_p^2}{\omega_{0i}^2 - \omega^2 - i\gamma_i \omega} \quad (8)$$

where ω_p depends on the density of bound electrons involved in the absorption process and γ is a damping constant for the bound electrons. This Lorentz model shows strong deviation from the free electron gas model near ω_0 , leading to a maximum in the imaginary part of $\epsilon(\omega)$ and strongly increased damping.

Au, Ag, Al and Cu are used as materials for metallic optical antennas. The dielectric constants of Au and

Cu are very similar, with a Drude-like response for wavelength above 600 nm and an onset of interband transitions occurring around 530–550 nm, making them excellent for antennas in the red and near-IR spectral region. For Ag the first interband transition is for a short wavelength, less than 400 nm, making it superior to Au for wavelengths around 500 nm. Al has a larger negative real part of dielectric function, and so among the four metals is the one that best approximates an ideal metal, especially in the 400–600 nm spectral region¹¹⁶. Unfortunately there is an interband absorption peak located at 800 nm wavelength, making Al unsuitable for use in the near-IR region, although, as previously discussed, it makes a good candidate for solar rectenna due to its high predicted matching efficiency⁹⁵. As well as the spectral properties of the metals, the chemical stability also needs to be carefully considered. Ag and Cu are known to rapidly oxidise under ambient conditions and Al forms thin passivation layers of Al_2O_3 . Due to its dielectric functions in the red and near IR parts of the spectrum and its excellent chemical stability, Au is the material most often used as a nanoantenna.

B. Scattering and Absorption Properties of Optical Antennas

Radio frequency and microwave antennas will normally always be considered as circuit elements connected to a feeding circuit. At optical frequencies the circuit element models are not valid and so optical antennas often appear as isolated or electromagnetically coupled structures, whose resonant properties have to be considered. Here, the LSPR of single and coupled metal nanoparticles, specifically the absorption and scattering properties, are considered. Consider a monochromatic plane wave of irradiance I_i incident on a sphere of radius a . If the irradiance is multiplied by a cross-section then the power absorbed or scattered by the particle can be calculated,

$$P_{abs} = I_i C_{abs} \quad (9)$$

$$P_{sca} = I_i C_{sca} \quad (10)$$

where C_{abs} and C_{sca} are the absorption and scattering cross-sections, respectively. The cross-sectional areas can be normalized to the cross-section of the sphere to give the scattering and absorption efficiencies:

$$Q_{abs} = \frac{C_{abs}}{\pi a^2} \quad (11)$$

$$Q_{sca} = \frac{C_{sca}}{\pi a^2} \quad (12)$$

where a is the radius of the sphere. Equations 11 and 12 define the two loss mechanisms, Q_{sca} which is radiative and Q_{abs} , which is non-radiative, the extinction efficiency

being the sum of both these terms.

Smaller sized particles restrict electron motion and cause electrons to collide with the inner surface of the particle, resulting in loss of energy and increased absorption. Absorption is therefore the greater loss mechanism in smaller particles. The radiation damping rate is proportional to the number of electrons. This means that the larger the particle, the more significant this factor and the broader the plasmon resonance becomes. A larger particle volume results in a decrease in the amount of incident radiation absorbed but an increase in the scattering. Scattering and absorption due to small spheres can be described using the well-known Mie theory¹²¹, where

$$C_{abs} = \frac{2\pi n_1}{\lambda_o} Im(\alpha) \quad (13)$$

$$C_{sca} = \frac{\left(\frac{2\pi n_1}{\lambda_o}\right)^4 |\alpha|^2}{6\pi} \quad (14)$$

The polarization, α , is given by:

$$\alpha = r^3 \frac{(\epsilon_2 - \epsilon_1)}{(\epsilon_2 + 2\epsilon_1)} \quad (15)$$

where r is the radius of the sphere, ϵ_2 the complex permittivity of the sphere and ϵ_1 the complex permittivity of the surrounding medium. Examples of Mie theory calculations of extinction, scattering and absorption for gold and silver spheres of various radii are shown in Figure 10.

Interesting observations that arise from the Mie theory calculations are that a number of peaks can be observed for larger diameter spheres, the longest wavelength peak being a dipole mode. As expected the LSPR broadens as the particle size increases but absorption and scattering maximums are not always at the same wavelength. The absorption and scattering properties can be tuned using different shaped particles. In this case more complex calculation methods are required, for example the Discrete Dipole Approximation (DDA)¹²³, Finite Element Method (FEM)¹²⁴ or Finite Different Time Domain (FDTD)¹²⁵. FDTD is a popular method since it is possible to consider the scattering and absorption from any shaped particle in any dielectric environment and since the calculation is in the time domain a single calculation will yield the spectral response over a wide bandwidth, using a Fourier Transform¹²⁶.

If a surface that fully encloses the scattering object is now defined, then by considering the total field flowing through it, one can calculate the normalized absorption cross-section Q_{abs} from¹²⁷,

$$Q_{abs} = \frac{\int Re(0.5\mathbf{E} \times \mathbf{H}^*) d\mathbf{a}}{|S_i|} \quad (16)$$

and by considering the scattered field the normalised scattering cross-section, Q_{sca} , is found from¹²⁷,

$$Q_{sca} = \frac{-\int Re(0.5\mathbf{E}_s \times \mathbf{H}_s^*) d\mathbf{a}}{|S_i|} \quad (17)$$

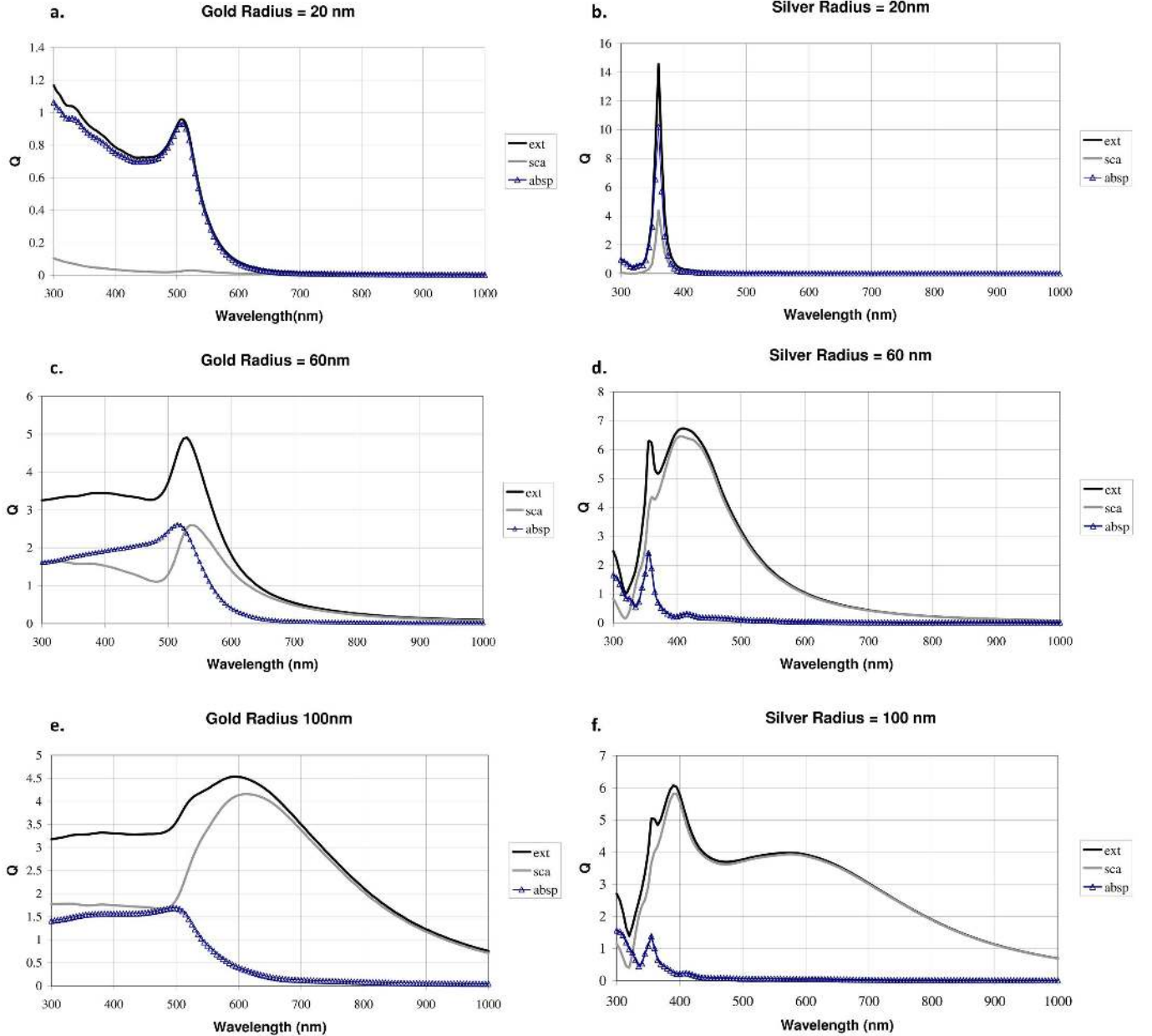


FIG. 10. Mie calculations of extinction, scattering and absorption efficiencies for silver and gold nanospheres (a) Au sphere of 20 nm radius (b) Ag sphere of 20 nm radius (c) Au sphere of 60 nm radius (d) Ag sphere of 60 nm radius (e) Au sphere of 100 nm radius (f) Ag sphere of 100 nm radius.

where $|S_i|$ is the power incident on the cross-sectional area of the nanoantenna. Using computational electromagnetics to calculate the electric (\mathbf{E}) and magnetic (\mathbf{H}) fields at the enclosing surface, Equations 16 and 17 can be solved. Figure 11 shows the Q_{sca} calculated using FDTD for (a) two closely spaced and (b) two overlapping spheres, where the spheres are silver and of 50 nm diameter¹²².

Furthermore, the surrounding dielectric environment and orientation of the nanoparticle can significantly modify the absorption and scattering properties¹²⁷. As an

example, consider the two configurations of 30 nm radius hemispherical Au nanoparticles, depicted in Figure 12. In both configurations the metal nanoparticle is at the interface between the air and silicon on the lower surface of the semiconductor. In the first case the nanoparticle extends into air whilst for the second case it extends back into the silicon. In each case the scattering properties of the metal nanoparticle are calculated when there is a normally incident field from within the silicon¹²⁷. The results are shown in Figure 13. It can be seen that in case (b) the scattering efficiency is dominant whereas in

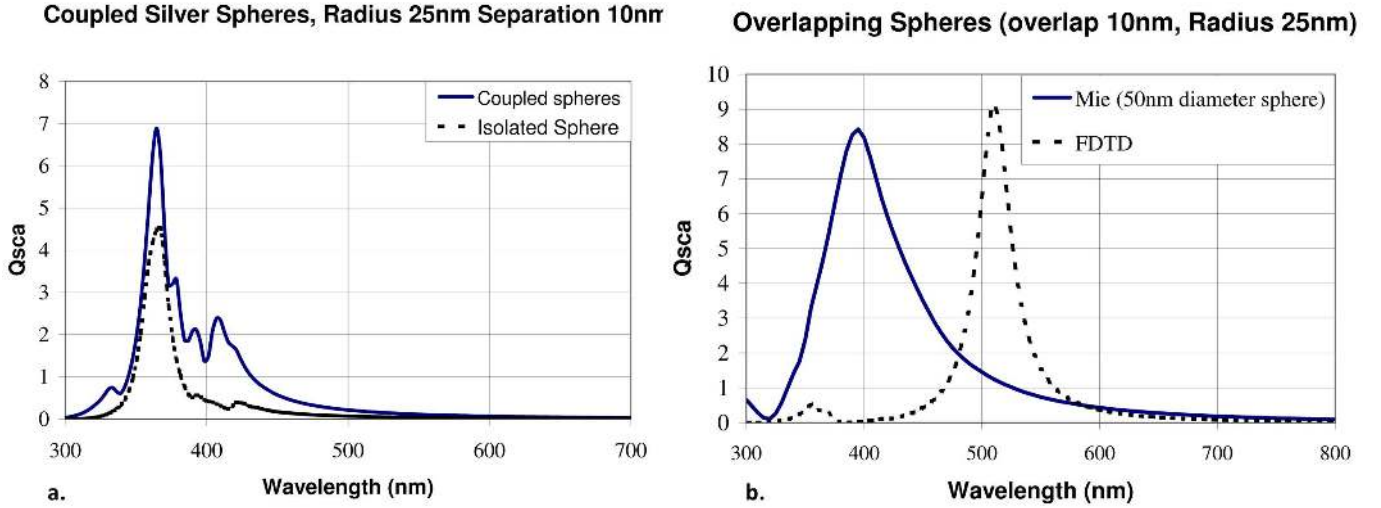


FIG. 11. FDTD calculations of Q_{sca} for (a) two closely coupled Ag spheres and (b) two overlapping Ag spheres.

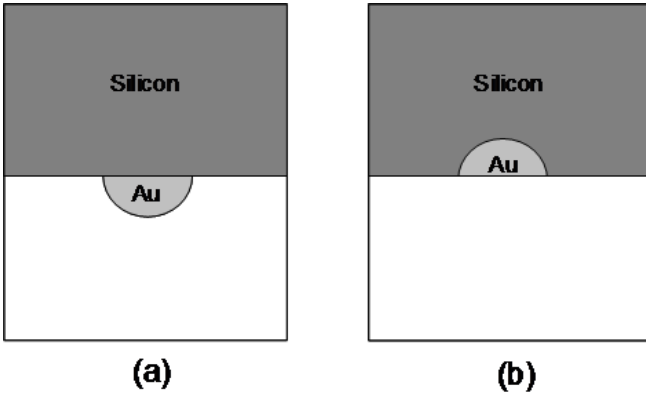


FIG. 12. Depiction of the two configurations considered: (a) nanoparticle extending into air and (b) nanoparticle extending into silicon. (Reprinted from [127])

case (a) it is the absorption that is the largest extinction component.

We have discussed the LSPR of isolated and coupled nanoparticles in terms of their absorption and scattering efficiencies. The subsequent coupling between the nanoantenna and rectifying diode will need to be optimised. Absorption is caused by the generation and recombination of electron hole pairs (EHP). EHP formation occurs when the plasmon quantum excites an electron from the Fermi level to an occupied state below the vacuum level. It has been shown that the concentrated electric fields around a nanoantenna, due to the LSPR, can cause hot electron carriers^{128–130}. Because of their higher energy, hot electrons will extend further away from the nanoparticle than an equilibrium electron distribution, which is above the vacuum level. If a nearby electron ac-

ceptor is present, hot electrons can transfer into its electronic states. This hot electron carrier generation and injection into an acceptor due to the high fields is a topic of much current research in photovoltaic devices^{128–131}, in particular optimizing the efficiency of this process.

For an optical rectenna it is desirable to enhance and localize (i.e. concentrate) the propagating fields to enable coupling into external circuit elements. The concentrated fields tend to be higher for particles with a higher scattering efficiency and between the small gaps of coupled nanoparticles. This is opposite to hot electron devices which seek to maximise the absorption of photons in the nanoparticle. Figure 14 shows the values of electric field, normalized to the incident field, around Ag nanoparticles, formed by colloidal lithography using 500 nm polystyrene spheres as a template on a glass substrate¹³² (this makes the triangular sides around 120 nm in this case). The scale is logarithmic and it can be seen that there are up to two orders of magnitude electric field enhancement in the gaps between the particles.

C. Alternative structures

Progressing toward a more efficient energy harvesting technology, some creative and novel designs have been explored. Other than the hot electron assisted mechanism, the idea of optomechanical nanoantenna has also been explored. In this design, the plasmonic bowtie antenna when coupling with the incident radiation, generates a strong electric field in the gap regions of the antenna arms and bend the arms toward each other¹³³ (Figure 15). As the arm bends toward each other, a redshift in transmission and reflection power occurs, allowing the device to have a larger operation bandwidth. With the inclusion of surface plasmon polariton property, it is calculated that

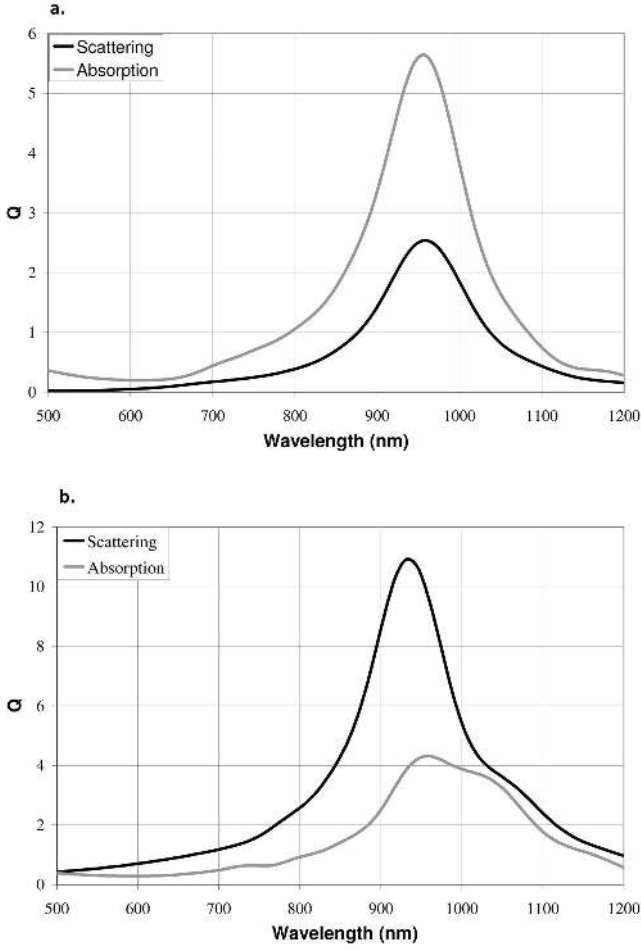


FIG. 13. Q_{sca} and Q_{abs} FDTD calculations for (a) nanoparticle extending into air (b) nanoparticle extending into silicon. (Reprinted from [127])

the antenna length can be greatly reduced while provide a mechanical bandwidth of 4.4 GHz.

The propagation wavelength for the waveguide in the material is very small. This suggests that if the antenna is very close to the diode, it can reduce losses¹¹⁶. In Travelling Wave (TW) MIM rectenna design, a MIM junction is created between the top and bottom bow-tie antenna^{134,178} (Figure 16a). This allows the diode to rectify the absorbed radiation at this MIM junction. This design is similar to a bow-tie antenna, except that the left bow and the right bow are separated by a very thin layer of insulator, forming an extended MIM tunnelling diode. The absorbed radiation excites surface plasmon and propagates along this axis (Figure 16c). The current induced between the top metal and bottom metal cause tunneling of electrons to occur. A final rectified current is produced due to the asymmetry in the IV characteristic at the bias point (further information in Section V). One of the advantage in this design is that it is not limited by the RC bandwidth.

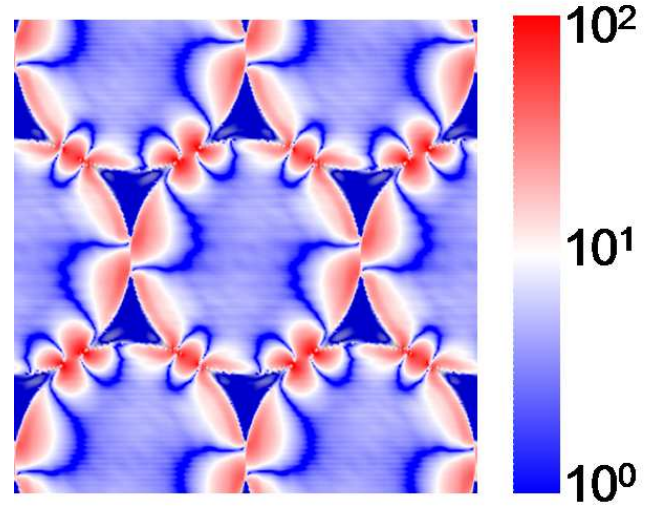


FIG. 14. Concentrated electric field calculations around triangular like nanoparticles of height 100 nm formed by colloidal lithography with 500 nm polystyrene spheres. The excitation wavelength is 780 nm and calculations were carried out using FDTD. (Reprinted from [132])

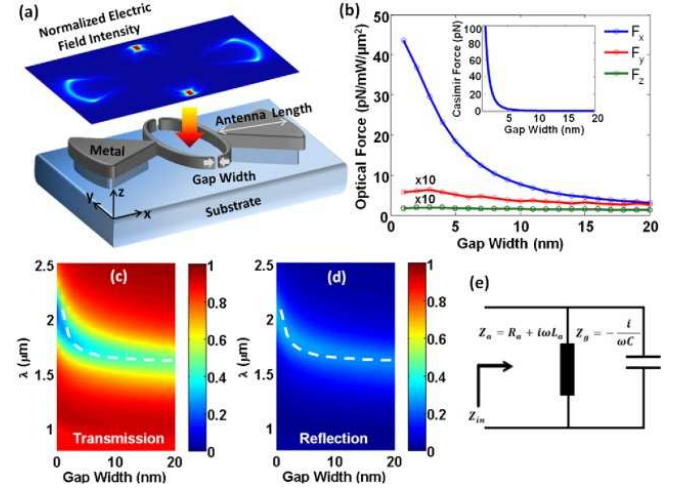


FIG. 15. (a) 3D schematic diagram of the optomechanical nanoantenna investigated. A near-field intensity map of the device is shown on top. (b) Simulated optical force and Casimir force (inset) on the suspended beam as a function of gap width. (c) Simulated (a) transmission and (b) reflection power spectrums versus gap width. (e) Nanocircuit lump elements model. (Reprinted from [133], ©2012 with permission from Optical Society of America)

Another example of integrated rectenna design is the slot-antenna-based frequency selective surface (FSS) with integrated MOM diode¹³⁵. The materials consists of Al, Al_2O_3 and Pt on benzocyclobutene (BCB) standoff, designed for absorbing radiation at 28.3 THz (10.6 m). Numerical simulations showed that when the incoming radi-

ation is parallel to the diode junction, the electric field is concentrated 2000 times across the diode with a decrease of reflectance around the desired wavelength, which can be used as an indication of absorption. A working device was fabricated with e-beam lithography (Figure 17) and similar optical response in reflectance was measured.

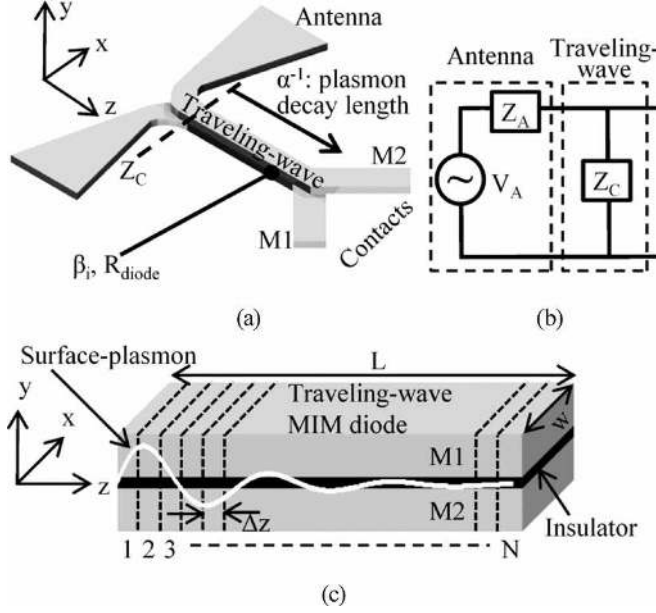


FIG. 16. (a) Isometric view of the antenna-coupled TW device. Instead of crossing over as in a typical bow tie antenna in figure 1, the antenna arms converge into a parallel-plate waveguide with a 2 nm thin insulator between the metal M1 and M2. (b) Circuit representing the TW MIM device. (c) 3D view of the TW MIM diode. (Reprinted from [134], ©2010 IEEE. Reprinted, with permission, from IEEE)

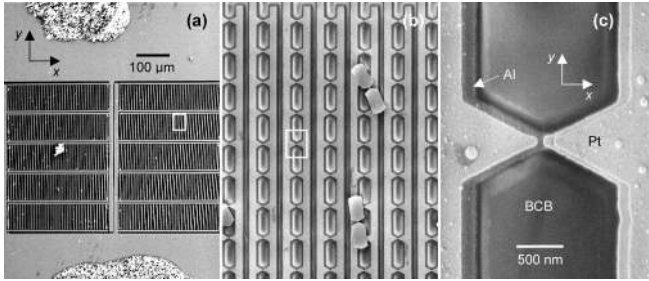


FIG. 17. SEM images of fabricated MOM diode-coupled frequency selective surface device. (a) Image of entire array consisting of 16,800 diode-coupled elements is less than 0.325 mm^2 , (b) closer image of the array showing several pieces of metal coated photoresist that became attached to the sample after lift-off, and (c) diode of working device (Reprinted from [135], ©2012 with permission from John Wiley & Sons)

The recent development of graphene technology also prompts the incorporation of graphene into nanoantenna

design. Ag is known to suffer from sulfidation under ambient environment, resulting in degradation of the plasmonic property¹³⁶. Graphene was shown to be able to passivate the Ag and prevent sulfidation without affecting the plasmonic property of the Ag nanoantenna¹³⁶. Additionally, radical changes in the plasmon energy and strength were also observed by electrically doping patterned graphene arrays with a gate voltage¹³⁷. The development of new materials such as graphene open up new possibility to design a better optical antenna.

D. Impedance matching

As previously introduced, the efficient energy transfer from antenna to diode requires an impedance match between both components. A theoretical analysis on an optical dipole nanoantenna showed that the nanoantenna appears to be an effective RLC parallel circuit¹³⁸ (Figure 18). The two parallel resistances are due to radiative decay and non-radiative decay rates. The electrical properties of a nanoantenna are intrinsically influenced by the material used, dimensions and geometric shape⁹⁵. Dipole antennas of length between 100 and 350 nm for Ag, Al, and Au on glass have been studied through simulation⁹⁵, as previously introduced. At a single frequency and assuming no loss of power in impedance mismatch, a silver dipole shows the highest efficiency. However, the upper bound efficiency drops when the solar irradiance spectrum is taken into account. Further investigation by inclusion of losses due to impedance mismatching showed even further decrease in conversion efficiency (see Section III).

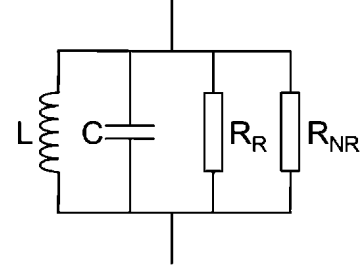


FIG. 18. Equivalent circuit of a metallic nanoantenna. (Reprinted (Fig. 1) with permission from [138], ©2010 by the American Physical Society)

Liu *et al.*¹³⁹ considered the nanoantenna as lumped elements in three-dimensional nanocircuits and demonstrated that impedance of the antenna can be tuned by loading a dielectric or a metal in the gap between a dimer. A SiO_2 load was used as the dielectric material. In the circuits it represents an additional capacitor for the dimer system. When gold is loaded between the gold dimers, the nanocircuit becomes an LC circuit. The gold load acts as an optical frequency inductor and the two gaps between the gold load and gold antenna behave as two

capacitors. To develop the idea further, a combined gold-SiO₂ load was also fabricated. The circuit now corresponds to an LC parallel circuit in series. In all cases, the impedance was tunable by changing the dimensions and the materials of the load, with the gold-SiO₂ showing largest tunability.

E. Nanofabrication

For microwave energy extraction device dimensions are in the micrometre range, achievable using well established photolithography techniques. At infrared and optical frequencies nanometre dimensions are required. Unfortunately the resolution of photolithography is limited by the diffraction wavelength of light and so different fabrication techniques are required. Fabrication techniques that have been demonstrated to be effective at obtaining nanometre resolution are electron beam lithography, nano-imprint lithography and colloidal lithography.

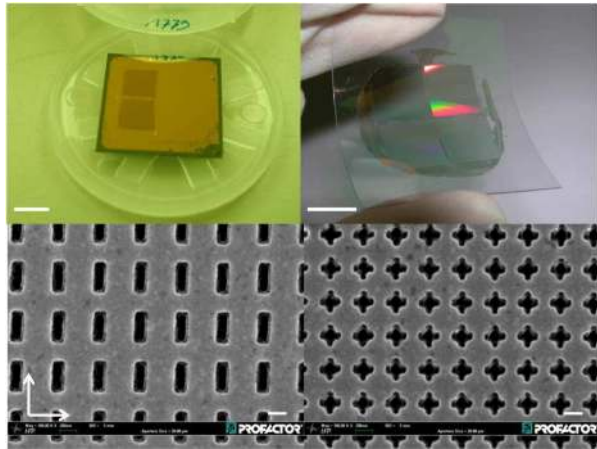


FIG. 19. (a) Photograph of a single layer negative index material (NIM) sample and (b) transfer printed gold grating on a flexible foil. Top-view SEM images of (c) the single functional fishnet layer and (d) the Swiss-cross NIMs fabricated using nanoimprint technology. (Reprinted from [141], ©IOP Publishing. Reproduced by permission of IOP Publishing. All rights reserved.)

Electron beam lithography is similar to photolithography but uses an electron beam instead of light. The wavelength of the electron beam is much smaller than light, allowing sub-10 nm resolution in patterning and creation of well-defined structure such as the nanogap in antenna-coupled diode in Figure 18. However it is costly and cannot be effectively up scaled for a large area. Nanoimprint lithography uses a pre-made mask to create a pattern on a substrate¹⁴⁰. This mask can be used numerous times and allows large area fabrication. Compared to e-beam lithography, nanoimprint lithography enables large area patterning but each mask is specially designed for a specific nanostructure. Figure 19 illus-

trates an example of a large area of nanostructures fabricated using nanoimprint technology. A new mask will have to be made if the nanostructure required is different and the cost of the mask is high. Nanosphere lithography is a more versatile lithography technique, based on self-assembly of nanospheres. It allows fabrication of large area devices at relatively low cost. Although it does not allow huge degree of manipulation in the shape of nanostructure compared to e-beam lithography, a variety of shapes in large ordered array has been fabricated successfully (Figure 20), such as nanotriangles^{132,142,143}, crescent moon¹⁴⁴, nanorings¹⁴⁴, nanocones¹⁴⁵, and three-dimensional structures¹⁴⁶.

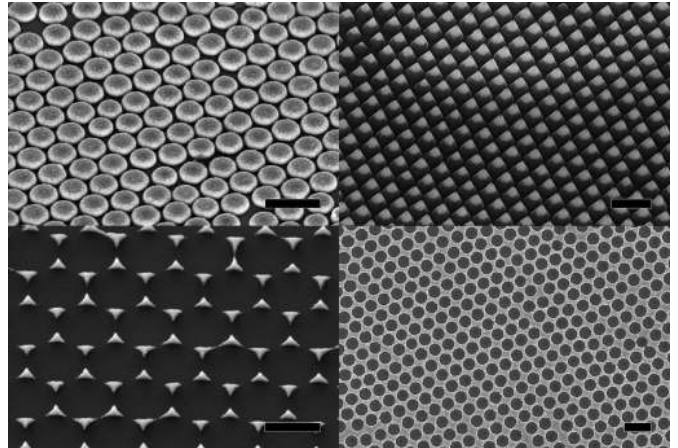


FIG. 20. SEM images of variety of gold nanostructures based on nanosphere lithography technique (a) nanotriangles, (b) slanted nanocones, (c) nanodisc array, (d) nanoholes. (Note: 500 nm scale bar in all images)

Advances in nanofabrication techniques are crucial in developing a better nanoantenna. Further details on nanoantenna theory and application can be found in some recent reviews [116,147].

V. RECTIFIER

A rectifier, a non-linear device such as a diode, is an integral part of the rectenna device, used to convert an AC input voltage from the antenna into a usable DC voltage. As discussed in Section III, the rectenna is fundamentally limited by the cut-off frequency (f_c) of the diode, above which the rectification process will become increasingly inefficient. f_c changes with the type of rectifier used due to the physical nature of the diode's operation dictated by its potential of achieving a low RC time constant. Schottky barrier diodes have been demonstrated and are theoretically limited to frequencies of a few THz, whereas MIM/MIIM diodes are shown to be operational at 150 THz^{5,148} and are predicted to potentially exceed this and reach the visible regime. Three

parameters have been defined^{5,149,185,188}, which, if satisfied, result in characterising a device as a diode rectifier:

$$f_{asym}(V) = \left| \frac{I_F(V)}{I_R(V)} \right|; \text{Asymmetry} > 1 \quad (18)$$

$$f_{NL}(V) = \frac{dI}{dV}(V) / \frac{I(V)}{V}; \text{Nonlinearity} > 3 \quad (19)$$

$$f_{RES}(V) = \frac{d^2I}{d^2V}(V) / \frac{dI}{dV}(V); \text{Responsivity} > 7V^{-1} \quad (20)$$

These three Figures of Merit (FOM) are commonly used to characterise the performance of MIM devices however can be equally applied to other diodes. The asymmetry FOM, defined in Equation 18, is the absolute ratio of forward to reverse current at a bias, a value of 1 indicating full symmetry and hence no rectification. The non-linearity FOM, as defined by Equation 19, is the ratio of the differential conductance to the conductance and is a measure of the deviation from a linear resistor. Finally the responsivity FOM defined in Equation 20 is the ratio of the second derivative of the I-V curve and the differential conductance and is a measure of the rectified signal as a function of input power. It is essential that the diode in a rectenna exceeds all of these criteria as the higher the FOMs for the diode, the more efficient the rectification process.

note: There was some disagreement argued by Tucker & Feldman¹⁵⁰ that responsivity should be described using second-difference equations and not derivatives in order to understand high frequency rectification. However, proving which is the correct approach is beyond the scope of this review as the authors aimed to only bring this theory to the attention of readers. The authors support the use of derivatives of the I-V curve in analysis of these FOMs.

The fundamental operational theory and recent experimental and theoretical developments of Schottky barrier diodes (used in the microwave power transmission rectenna), metal-insulator-metal and metal-insulator-insulator-metal diodes (proposed for solar rectenna), and geometric diodes (proposed for solar rectenna) will be reviewed in this chapter.

A. Schottky Barrier Diodes

Schottky barriers have been used as rectifying devices since the first cat's whisker detectors in the first decade of the 20th century. The 'barrier' itself is formed within the semiconductor side of a metal-semiconductor (MS) interface, the result of its conduction and valence bands bending to align the Fermi levels of each material. Figure 21 shows an ideal MS interface with the Schottky barrier, $\Phi_{B,n}^0$, marked.

In Figure 21, note that within the semiconductor, a

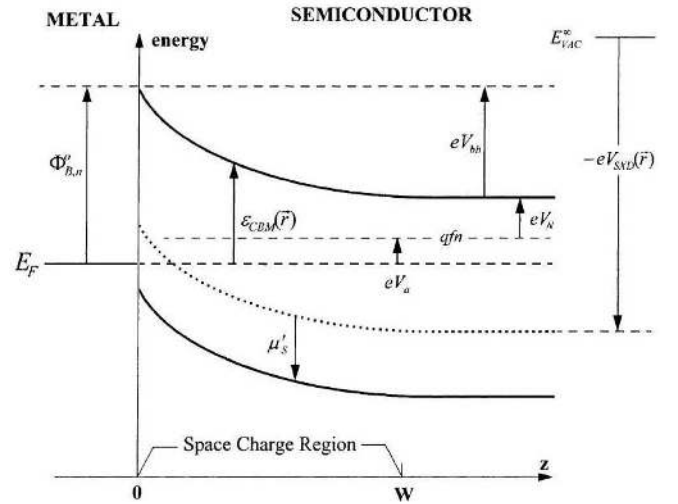


FIG. 21. Band diagram of an ideal Schottky Barrier, $\Phi_{B,n}^0$, contact formed with n-type semiconductor with an applied bias, V_a . (Reprinted from [151], ©2001 with permission from Elsevier)

depletion region, or space charge region, forms. This is a region of the semiconductor that is devoid of mobile charge carriers when the device is unbiased, and as such it can be considered as the dielectric between two plates of a capacitor, so having a direct influence on the RC time constant. Minimising the capacitance of a Schottky diode can be achieved through scaling (though this has the equal and opposite effect on the diode's resistance), or by increasing the depletion region width by using low semiconductor doping.

The full operation of a diode has been well studied and understood over the past century, and readers are referred to [152,154], for a basic understanding of Schottky diode formation, operation and physics under different biasing conditions. Both the forward and reverse current-voltage (I-V) relationship is in most cases, where semiconductor doping is low enough, dictated by thermionic emission, rather than recombination or tunneling. The equation for thermionic emission, where the carrier in the semiconductor must pass up and over the potential barrier into the metal, is classically expressed as^{152–154},

$$I = AA^*T^2 \exp(-\beta\Phi_{B,n}^0) [\exp(\beta V_A/\eta) - 1] \quad (21)$$

where A represents the contact area, A^* is the Richardson constant, T is the temperature, V_A is the applied voltage, η the ideality factor and $\beta = q/k_bT$, with q the electron charge, and k_b the Boltzmann constant. However, built into Equation 21 is the presumption that a perfect, homogeneous interface exists, with just one uniform value of $\Phi_{B,n}^0$. Instead, a more realistic scenario should be considered where multiple current paths exist flowing over barriers of different barrier height, so modifying this equation that has been the standard for a century or more. The papers by Tung^{151,160} and others^{155–159} pro-

vide a much more rigorous understanding of the Schottky diode and its operation under this inhomogeneous regime. Given the small potential size of a Schottky rectenna, the impact of such interface inhomogeneity will be the source of significant device-device variation, and an unpredictability of cut-off frequencies.

Typical Schottky diodes can have good diode characteristics in terms of the FOMs mentioned in Equations 18, 19 and 20, as demonstrated by the simple example of a Cr/Si Schottky diode made in-house for [155]. The characteristics of this diode are close to ideal (i.e. $\eta < 1.1$), and its FOM values are strong, with a diode asymmetry of 1669, nonlinearity of approximately 0.2 and responsivity above 10 V^{-1} . However, high series resistance and depletion region capacitance result in a cut-off frequency of just 40 GHz. Therefore, this is a device which could be suitable in a microwave power transmission rectenna, but it would be entirely ineffectual at solar frequencies.

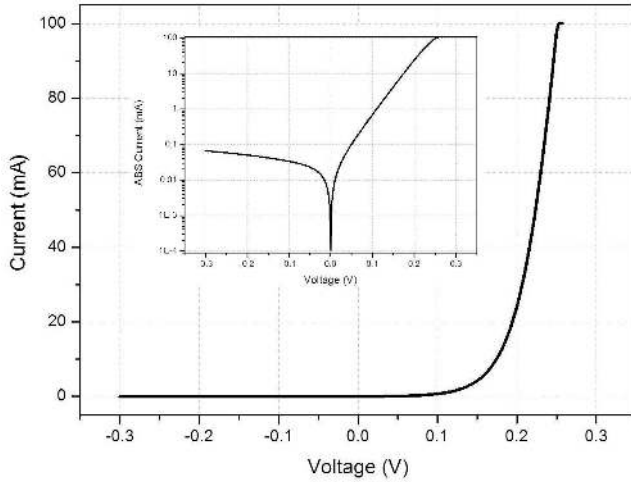


FIG. 22. Room temperature Current-Voltage characteristics of a simple Cr/n-Si lateral type Schottky barrier diode of area 0.448 mm^2 . SBH calculated at 0.51 eV , ideality factor of 1.06, diode asymmetry at $\pm 0.25 \text{ V}$ of 1669, nonlinearity estimated at 0.2 and responsivity above 10 V^{-1} . The cut-off frequency has been estimated at 40 GHz.

With appropriate device design in terms of size and interface homogeneity, parasitic capacitances and resistances, arising from skin effects and residual native oxide scales at the MS interface, can be minimised to have a significant effect on the RC time constant. In silicon the cut-off frequency has been seen to reach 1 THz obtained by a layer of Ti-Pt-Au on a thin layer of n-Si¹⁶¹, whereas 400 GHz has been seen from a simple Ti/n-Si structure¹⁶². On GaAs, frequencies of up to 5 THz have been achieved, as reviewed by Sizov & Rogalski¹⁶³. This is obtained using highly doped GaAs substrate with an Ohmic contact on the back side upon which a thin ($0.3\text{--}1 \text{ }\mu\text{m}$) epitaxial GaAs layer is grown, with Pt forming the Schottky contact. A honeycomb diode chip design

enables thousands of diodes (diameters of $0.25\text{--}1 \text{ }\mu\text{m}$) on a single chip whilst minimising parasitic losses.

As rectifiers in the wireless power transmission rectenna application, SBDs are more than suitable candidates and as seen in Section III can operate efficiently. With cut-off frequencies in the low THz, Schottky diodes may potentially find usage as infrared rectennas although they will be limited to only function at a fraction of the far-infrared range, where the incident solar radiation is only up to $0.3 \text{ W/m}^2/\text{nm}$. The aim is to have solar rectennas operating at the high THz region where solar radiation is up to $1.7 \text{ W/m}^2/\text{nm}$, however Schottky diodes will not be able to efficiently rectify such high signals. Therefore, other approaches such as the MIM/MIIM and geometric diodes are being considered for the solar rectenna.

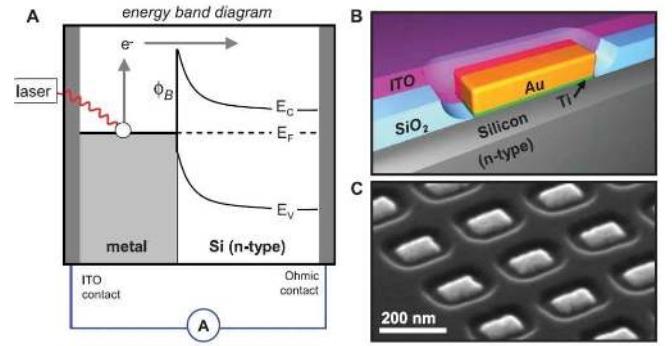


FIG. 23. Schottky diode as the active component for the solar rectenna device - concept inspired by Knight *et al.* **A** showing a band diagram of the proposed photocurrent mechanism, **B** showing the device layout and structure and **C** showing an SEM image of the array of devices. (Reprinted from [94], ©2011 with permission from The American Association for the Advancement of Science)

An alternative approach, which was first proposed by Knight *et al.*⁹⁴, is to use the diode as the active component in a hot-electron device. In this case, the array of nano-metre scale anodes double as the antennas, in which the incident light causes a localised surface plasmon resonance. Plasmon decay produces electron-hole pairs and as represented in Figure 23A, hot electrons are injected into the semiconductor after overcoming the Schottky barrier energy. The reported⁹⁴ quantum efficiency of this structure is estimated at being just 0.01%, though improvements are suggested to reach efficiencies of 2%. Recent publication suggests 30% efficiency of converting “hot electrons” in the metal to electrons in the semiconductor¹⁶⁴, though full conversion efficiency has not been estimated. In this case, although the device is based on an antenna coupled to a rectifier (similar components to a rectenna), the device is not proposed for light harvesting purposes due to its low efficiency and is instead demonstrated as a photodetector. Development of this concept into an energy harvesting applications

would require the conversion efficiency to be increased, though with the current state-of-art, this seems improbable.

B. Metal-Insulator-Metal Diodes

Current transport in Metal-Insulator-Metal (MIM) diodes is due to quantum electron tunnelling through an ultra-thin insulator layer (typically < 10 nm¹⁶⁵). Rectification in these devices is due to variation in tunnelling rates caused by barrier asymmetry due to material selection, device geometry, thermal asymmetry, and photon induced deviation in electron flux distribution across occupied and unoccupied states¹⁰⁵, all contributing towards a nonlinear asymmetric I-V response. In the current review, we will qualitatively explain the nature of the I-V asymmetry taking into account the material selection for planar MIM devices under no illumination and thermal equilibrium. Under illumination, electron tunnelling is stimulated by different processes depending whether an antenna is or is not coupled to the diode. Further reading is suggested in [105,165,166,169]. Thermionic emission also contributes to tunnel diodes' I-V curves^{165,188,189}, especially to devices with thick insulating layers¹⁸⁸.

1. Theory of operation

Consider a Metal-Insulator-Metal junction as shown in Figure 24a. Metal 1 has a workfunction, Φ_1 , lower than that of Metal 2, Φ_2 , and χ is the electron affinity of the Insulator. The barrier height at the metal-insulator interface is determined from the difference between the workfunction and electron affinity respectively. At zero bias the band structure is shown in Figure 24a. By applying a negative bias (Reverse bias) to Metal 1, the band diagram shifts as in Figure 24b. In this case direct tunnelling is observed as a result of the *effective* tunnelling distance, d_t , being the same length as the insulator thickness. Further increasing the applied voltage, V_A , decreases the *effective* d_t , and it becomes shorter than the length of the insulator (as seen in Figure 24c). In this case, Fowler-Nordheim tunnelling¹⁶⁷ starts to occur. When a bias of the same magnitude is applied to Metal 2 (Forward biasing), the bands shift as in Figure 24d. Fowler-Nordheim tunnelling is observed in this case and occurs at a lower voltage, the higher the barrier asymmetry at both metal-insulator interfaces (arising from the difference in metal workfunctions). Further increasing the reverse bias (as in Figure 24e) will further decrease the *effective* tunnelling distance, d_t , which further increases the tunnelling probability in forward bias. Therefore, rectification occurs because for the same voltage magnitude in forward bias, d_t will be shorter and more current will be flowing than in the equivalent case in reverse bias. By changing the applied voltage, the tunnel distance changes linearly and the tunnel current is ex-

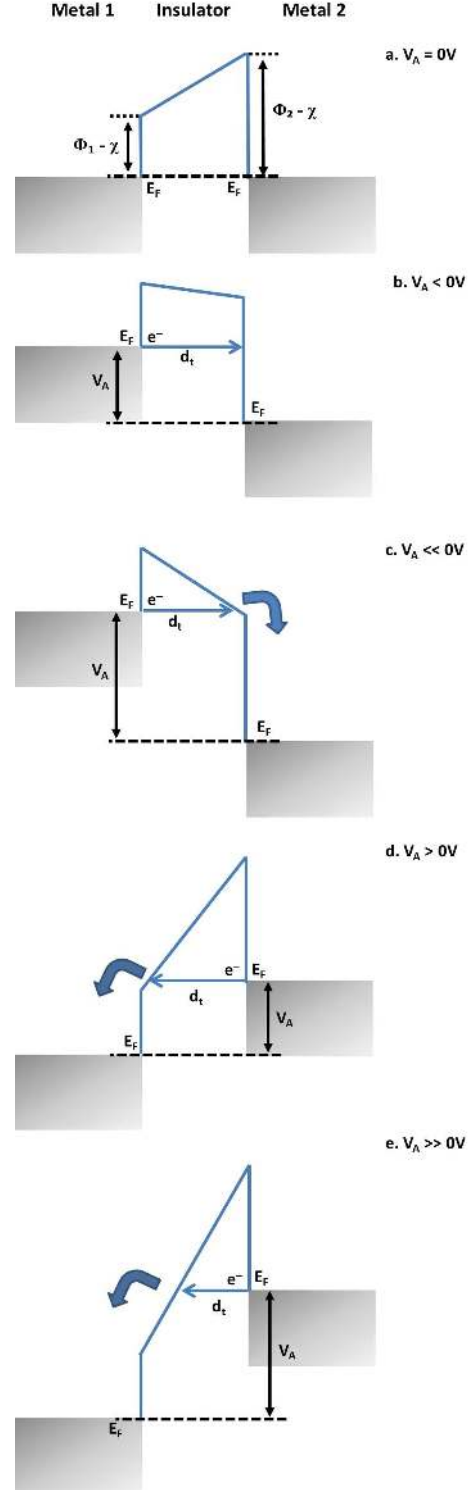


FIG. 24. Ideal band diagram for a MIM diode with dissimilar workfunctions for Metal 1, Φ_1 , and Metal 2, Φ_2 , χ the Insulator's electron affinity, E_F the Fermi level, d_t the tunnel distance and V_A the applied voltage. **a.** No bias situation ($V_A = 0V$); **b.** & **c.** Negative bias at Metal 1 (Reverse bias); **d.** & **e.** Positive bias at Metal 1 (Forward bias).

ponentially dependant on this distance¹⁶⁸. This leads to an asymmetric, nonlinear current-voltage response and is the origin of the rectification mechanism in MIM diodes.

2. Experimental devices

Various metal-insulator systems have been used to investigate the rectification behaviour of MIM diodes. Research attempts are concentrated either towards modelling the behaviour and rectification properties or improving the figure of merits by optimising the material selection and fabrication techniques of these structures. As theory suggests, using similar metals in the MIM configuration should yield symmetric I-V curves, however asymmetric I-V curves have been reported for Al/Al₂O₃/Al¹⁷⁰ with structures and experiments conducted by the authors on Ti/TiO₂/Ti and Nb/Nb₂O₅/Nb devices having also displayed asymmetric I-V curves for these structures. The origin of this asymmetry is suspected to come from the formation of two different metal-insulator interfaces arising from dissimilar deposition processes, thus creating regions of enhanced leakage currents through the barrier. Other reported structures with optimised oxide layers such as Ni/NiO/Ni^{108,174,176–178,180}, Al/Al₂O₃/Al¹⁷¹ and Nb/Nb₂O₅/Nb^{149,185,187} show symmetry in the I-V curves, which is compliant with theoretical predictions. Although not displaying rectification properties, the Ni/NiO/Ni system is widely used for detection and mixing up to 30 THz infrared radiation due its significantly low resistance-area product of $1 \Omega(\mu\text{m}^2)$ ^{108,176–178}, which indicates the potential for a low RC constant. However due to a lack of asymmetry, the second Ni electrode must be replaced with a metal of different workfunction in order to achieve rectification. This has been investigated by Hoofring *et al.*¹⁷⁵, Krishnan *et al.*^{111,179} and Esfandari *et al.*¹⁸¹ with Au, Cr and Pt contacts respectively, all displaying good asymmetrical I-V response. Other structures of dissimilar materials which have shown promising results are Al/Al₂O₃/Ni¹⁷², Nb/Nb₂O₅/Pt^{149,184,185}, ZrCuAlNi/Al₂O₃/Al¹⁸² and also Nb/Nb₂O₅/Ag (tested in-house and by [190]). More tested metal-insulator combinations are listed in [149].

ZrCuAlNi was suggested as an electrode due to its low roughness after growth, making it suitable for MIM devices^{182,183}. However, it is not ideal due to formation of an interfacial compound at the interface with the insulator. This was highlighted by Grover & Moddel¹⁶⁸, who anticipated the importance of material selection for a good MIM and that arbitrary combinations of metals and oxides are not always feasible, as for example Al/Al₂O₃/Pt¹⁷³ displays a linear I-V and yet has been successfully shown to work in an antenna-coupled infrared detector. A study by Heiblum *et al.*¹⁷⁴ tested Al/Al₂O₃/Al, Cr/Cr₂O₃/Au, Al/Al₂O₃/Ag and Nb/Nb₂O₅/Au MIMs by exposing them to an IR laser and concluded their poor rectification properties due to the production of large thermal contributions when ex-

posed to laser radiation. This is a very useful approach, which must be applied to other MIM candidates for solar applications. An alternative concept was previously described (Figure 16), consisting of a MIM diode based on a travelling-wave structure, which although having a symmetrical configuration (Nb/Nb₂O₅/Nb), outperforms planar type MIM diodes by three orders of magnitude at μm wavelength¹³⁴.

One of the most important findings in this field is a method for characterising the electrical properties of MIM devices by nanoindentation and later a bent wire technique suggested by Periasamy *et al.*^{149,184–187}. The concept is based on a metal being deposited on a silicon substrate, after which a continuous oxide is grown and the second electrode is a bent wire of a desired material. This ensures a small contact area and the ability to characterise a point-contact type MIM junction. This work is very useful as it gives the chance to study various metal-insulator combinations before attempting to optimise planar thin-film diode devices. This technique was used to systematically study the influence the metal workfunction difference has on the electrical properties of MIM diodes (reference [149]). The structures analysed have a Nb bottom electrode, Nb₂O₅ insulator grown by anodic oxidation, and eight different metal 2 selections (Hf, Zr, Nb, Ti, Cu, Ag, Au, and Pt). The result was that the workfunction difference has a direct influence on rectification properties, with the asymmetry increasing sharply for $\Delta\Phi > k_B T$. This agrees with theoretical predictions and with the models by Simmons¹⁹¹. Conversely, nonlinearity FOM displayed no direct correlation with $\Delta\Phi$. The highest FOMs were observed for Nb/Nb₂O₅/Pt, which displayed 1500 asymmetry, 4 nonlinearity and 20 V^{-1} responsivity meeting the criteria outlined in Equations 18, 19 and 20. Recently, this work was continued through (reference [188]) the fabrication of $6400 \mu\text{m}^2$ planar devices with the same Nb/Nb₂O₅ base and six metal top contacts (Ag, Cu, Nb, Ni, Au and Pt). The work confirmed a direct linear relation between increasing asymmetry and increasing $\Delta\Phi$ with Nb/Nb₂O₅/Pt showing optimal results with figure of merits of 7742 asymmetry, 4.7 nonlinearity and 52.2 V^{-1} responsivity. These are to our knowledge the largest FOM values recorded and hence the most promising structure to be successfully integrated into a solar rectenna.

Periasamy *et al.*¹⁸⁵ also characterise other oxides with a Nb metal base and Pt bent wire and prove a hypothesis whereby the best rectification properties are expected from using dissimilar metals and low barrier heights at each metal-insulator interface in order to sooner promote the faster Fowler-Nordheim tunnelling in the forward direction. To achieve smaller barriers, high electron affinity insulators must be selected. Due to this reason, Nb₂O₅ and TiO₂ outperform Al₂O₃ and MgO. Another requirement for the insulator is a large dielectric constant since for small area devices the capacitance is reduced, however due to the requirements for tunneling the ultra-thin

thicknesses in turn increases capacitance, which has to be kept to a minimum as per Equation 2.

3. Modelling approaches

Modelling MIM devices is a significant challenge due to the many practical aspects of such ultra-thin layers. Interface roughness, pinholes and fabrication anomalies may all adversely influence device performance, and are difficult to account for reliably in the models. Nevertheless, modelling MIM performance is essential in order to confirm established experimental results and fully understand device operation as there is always room for improvement. Simmons¹⁹¹ first proposed a model incorporating the WentzelKramersBrillouin (WKB) approximation, which is frequently used to reproduce MIM I-V curves. This model is very good at predicting forward characteristics, however it overestimates currents passing in reverse bias, leading to close to symmetric simulated I-V curves for dissimilar metal electrodes. Eliasson¹⁶⁵ developed a comprehensive model to predict rectification efficiency, tunneling transmission probability and estimation of device resistance in thin MIM diodes, with the exception of image forces and effective mass. Recently Hashem *et al.*¹⁹² developed more accurate models to simulate the I-V curves and figures of merit of MIM devices. The model can be used for multiple insulator layers, whereas Simmons model is only limited to single insulator predictions. These models were shown to accurately trace experimental results reported by Choi *et al.*¹⁹³ (on a polysilicon/SiO₂/polysilicon tunnel diode) whilst Simmons simulations predicted almost linear behaviour. With double insulator devices, the models are accurate in forward characteristics, however slightly underestimate the leakage currents in reverse bias. Recent work by Cowell III *et al.*¹⁹⁴ has developed a model to estimate the barrier height formation and tunneling effective mass of a MIM diode exhibiting Fowler-Nordheim tunneling, which can be used to help assess the impact of different processing conditions on the performance of the device.

4. Fabrication and Characterisation

Apart from material selection, the fabrication techniques used to manufacture MIM devices are also important for good device performance. Metal deposition is commonly deposited by sputtering or evaporation, techniques which are well understood, give high quality thin films and are industrially scalable. Controlled deposition of the ultra-thin insulator required for tunneling is a challenge. Anodic oxidation^{149,185,188} of the first metal electrode is a good way of controlling growth of a high quality oxide, however, it is limited to only being able to grow the derivative oxide of the underlying metal. For research purposes, pulsed-laser deposition (PLD) sup-

plemented by reflection high energy electron diffraction (RHEED)^{195,196} can be used for monolayer controlled growth of oxide layers. This technique achieves ultra-thin continuous stoichiometric films of extremely high qualities, however PLD is not industrially scalable. Alternatively, reactive magnetron sputtering may be used, but there is some uncertainty over the stoichiometry and thickness control when depositing insulators. One of the most promising growth techniques is atomic layer deposition (ALD), which is a self-limiting deposition process allowing accurate thickness and stoichiometry control similar to RHEED PLD whilst maintaining a comparably high throughput and possibility of industrial scale processing.

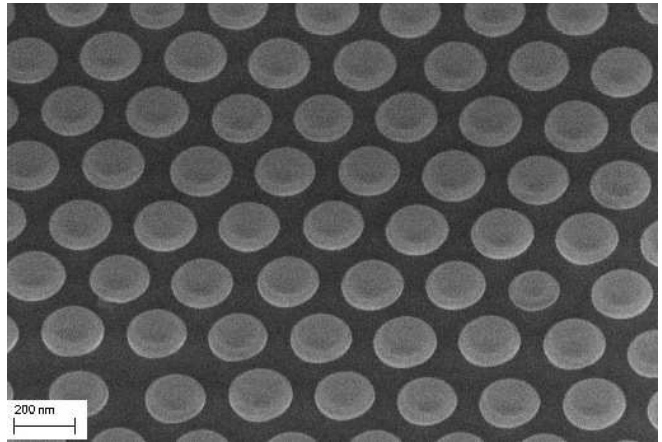


FIG. 25. SEM image showing an array of nanodiodes produced by growing a MIM multilayer, followed by colloidal lithography and Ar ion milling.

MIM device arrays of nanometer gap junctions over cm² areas¹⁰⁵, to create metal-vacuum-metal tunnel junctions which have similar properties to MIM diodes, also present a fabrication challenge. Common lithographic techniques have been used, but the economically viable techniques are limited to micron scale devices. However when the common lithographic techniques are supplemented by a recently optimised selective area atomic layer deposition technology¹⁹⁷, tunnel junctions of approximately 1 nm can be produced. This enables designs of antenna-rectifier coupled devices other than the more common planar types, which have great potential for success (see Miskovsky *et al.*^[105]). Another challenge is fabricating arrays of nano-scaled lateral diodes to be of the same size scale as required for high frequency antennas. Bareib *et al.* have developed a highly efficient method for producing an array of several million nanodiodes by temperature-enhanced transfer printing¹⁹⁸. These devices were characterised with a conductive atomic force microscope setup (C-AFM), which showed good asymmetry in the I-V response of the nanodiodes. An alternative technique was developed by the authors, which involves the deposition in a vacuum of the full MIM layers, fol-

lowed by colloidal lithography and Ar ion milling to give an array of nanodiodes (Figure 25), and preliminary C-AFM confirms assymetry.

Current MIM diodes remain limited to rectify the infrared part of the solar spectrum due to their RC time constant. In a study to confirm the applicability of MIM diodes to solar rectennas, Grover & Moddel¹⁶⁸ conclude that efficient coupling between antenna and rectifier must be achieved, which implies that the rectifier impedance must be around 100Ω as identified by Ma & Vandenbosch⁹⁵. Results by Chin *et al.*¹⁸⁸ show promising improvement in MIM performance, although the structure has a limited current density passing through it due to the relatively *thick* oxide used (15nm). MIM diodes appear to be a good candidate for the rectifiers in a solar rectenna and the ever increasing success in modelling, characterisation and fabrication of these multi-layered devices have shown their potential.

C. Metal-Insulator-Insulator-Metal Diodes

The addition of another Insulating layer was proposed as it would benefit the rectification properties of the tunnel diode. Using Metal-Insulator-Insulator-Metal (MIIM) devices, the diode figure of merits are improved over the single insulator case. Asymmetry here can be achieved even with similar metal electrodes, as long as the electron affinity of both insulators is different. For the purpose of understanding the concept, we will qualitatively explain the simple case of Metal 1 and 2 being the same and Insulator 1 having a higher electron affinity than Insulator 2. At zero bias the band structure is the one depicted in Figure 26a. When a negative bias is applied to Metal 1 the bands shift as in Figure 26b, where the *effective* tunneling distance, d_t , is of the length of both insulator thicknesses and direct tunneling through both insulators is observed. Increasing the bias will eventually shift the bands to the situation in Figure 26c and the d_t is now shorter, however the electrons will fall into the Quantum Well (QW), from where the tunneling probability is reduced. By reversing the bias, initially tunneling will be direct through both insulators as in Figure 26d. Further increasing the bias will shorten the *effective* d_t and the tunneling is again direct but through only one of the insulators (Figure 26e). Further increasing the bias will further decrease d_t by promoting Fowler-Nordheim tunneling, whilst in the reverse case electrons will continue to tunnel into the QW. The origin of the asymmetry in the I-V curves of MIIM diodes with similar metal electrodes is due to the shift in dominant tunneling mechanism during forward and reverse bias and the formation of the Quantum Well due to using insulators of dissimilar electron affinity. By employing different metal electrons, the rectification properties of MIIM diodes can be further improved.

If the thickness of the lower electron affinity insulator is increased relative to the other insulator then the

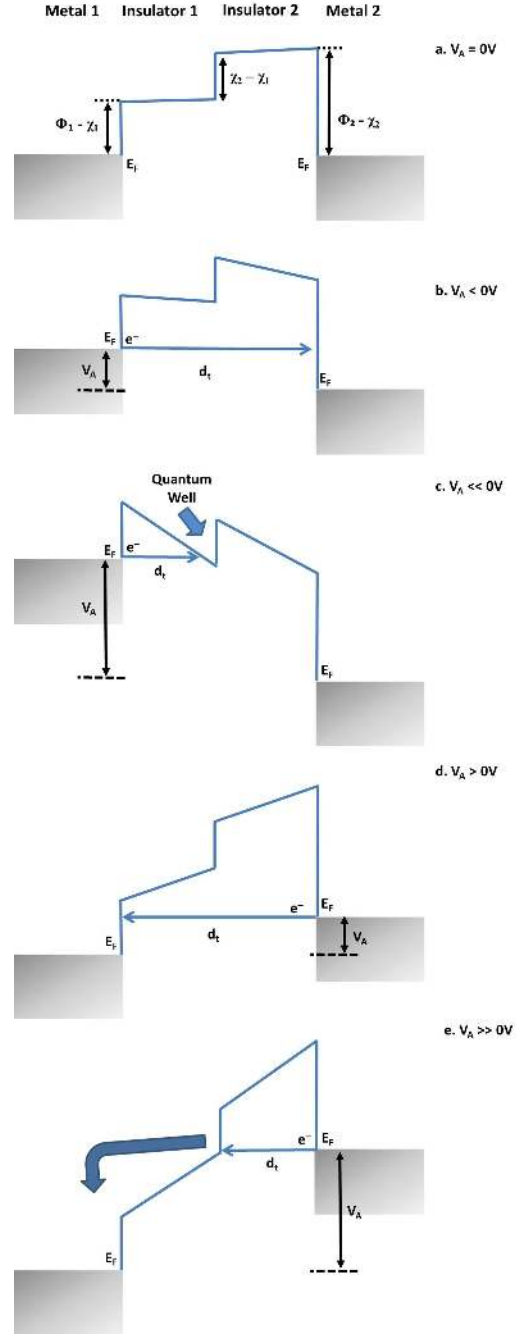


FIG. 26. Ideal band diagram for a MIIM diode with the same metal electrodes ($\Phi_1 = \Phi_2$) and two Insulators of equal thickness ($\chi_1 > \chi_2$). **a.** No bias situation ($V_A = 0V$); **b.** & **c.** Negative bias at Metal 1 (Reverse bias); **d.** & **e.** Positive bias at Metal 1 (Forward bias).

Quantum Well will be wide enough to form resonant energy levels^{199,200}. These quantised resonant tunneling energy levels have electron transmission probabilities higher than that for adjacent energy levels. Therefore, they introduce significant asymmetry into the I-V curve¹⁶⁵ in the opposite direction to the one which would be observed

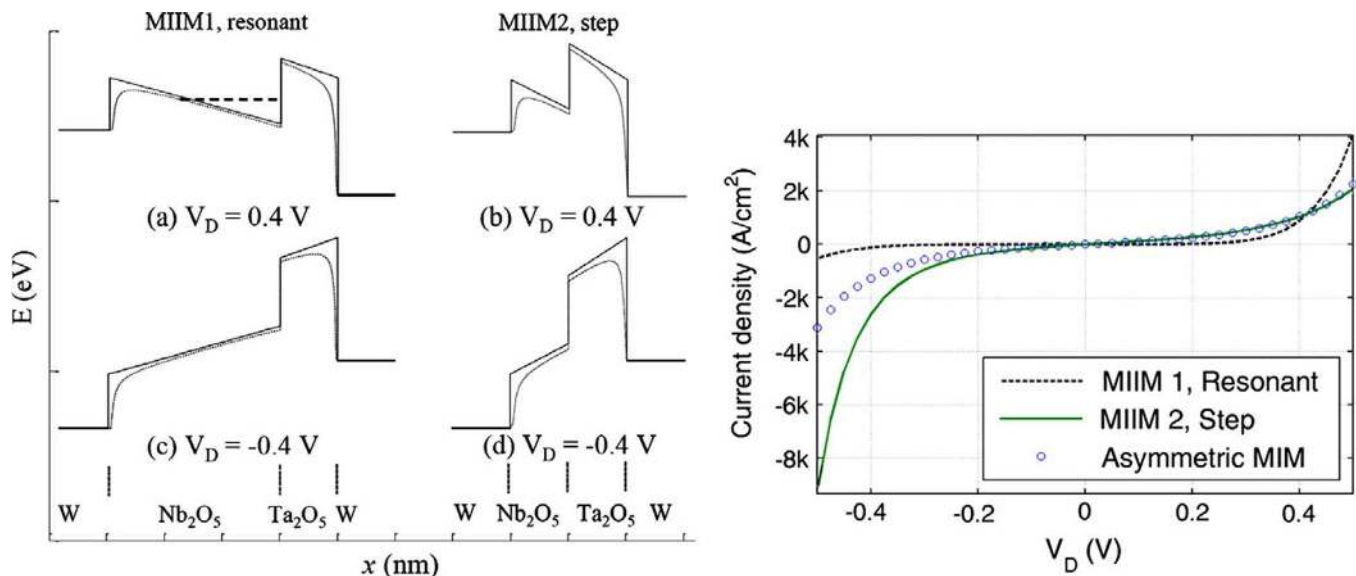


FIG. 27. Energy-band profiles for the W/Nb₂O₅/Ta₂O₅/W MIIM diodes discussed by Grover & Moddel (left) under forward and reverse bias for the resonant (a and c) and step (b and d) diodes, and their corresponding I-V curves also compared to an Asymmetric MIM diode (right). Notice how current enhancement for the resonant diode is in forward bias, whilst that for the step diode is in reverse bias. (Reprinted from [200], ©2012 with permission from Elsevier)

if no resonant tunneling states are present (step MIIM), as discussed and shown by Grover & Moddel²⁰⁰ (see Figure 27). Adding extra insulators with resonant levels further increases rectification²⁰¹.

MIIM devices were first introduced for solar based applications by Phiar Corp. and patented by Eliasson and Moddel^{202,203}. The performance of MIM and MIIM diodes as infra-red detectors was compared by Hegyi *et al.*²⁰⁴ by simulating their responsivity. It was shown that the MIIM diode has 10 times higher responsivity than a derivative MIM diode. This was experimentally shown by Maraghechi *et al.*²⁰⁵ who recorded up to 10 times better nonlinearity for a Cr/Al₂O₃/HfO₂/Cr diode compared to Cr/Al₂O₃/Cr and Cr/HfO₂/Cr diodes. A more applicable example, already referred to, is by Grover & Moddel²⁰⁰, who compared their W/Nb₂O₅/Ta₂O₅/W structure to an MIM Diode with equivalent barriers as that of a W/Nb₂O₅ on one side and a W/Ta₂O₅ on the other side, again clearly showing improved response from the MIIM device (Figure 27).

Material selection for MIIM diodes has similar criteria to that of MIM, in that the structure has to exhibit one kind of tunneling in one direction and another tunneling mechanism in the other, thus promoting highly asymmetrical nonlinear I-V curves. A significant challenge is fabricating two ultra-thin, stoichiometric, high quality insulators. The appropriate technique for research purposes is RHEED PLD, although ideally ALD would be the better option in terms of prospects for industrial scaling. Alimardani *et al.*^{206–208} have researched the use of ALD for depositing the double insulators required to produce efficient MIIM diodes. A recent patent²⁰⁹ proposes

the use of a triple-insulator barrier which adds further complexity to the fabrication process. The models created by Hashem *et al.*¹⁹² will help identify which material systems to concentrate experimental efforts on. Improved performance from multiple barrier tunnel diodes is yet to be realised but the few reports that exist suggest significant potential. Integration with antenna for solar rectenna would also have to be researched as the addition of extra insulators may have deteriorating effect on the *RC* constant preventing these devices to be used at high frequencies although their rectification properties are clearly superior.

D. Geometric Diodes

Geometric diodes are devices that display rectification properties due to the difference in charge carrier transport probabilities from one electrode to another as a result of a geometric constraint. An increasingly popular concept patented by Moddel²¹⁰ consists of a thin film patterned into an inverse arrowhead²¹⁴ configuration shown in Figure 28(a). The electrodes are placed on top of the thin film at both ends of the structure. The width of the neck, d_{neck} , is of the same magnitude as the mean-free path length (MFPL) of the thin film material in order to obtain rectification^{211–215}. Looking at Figure 28, an assumption is made by which charge carriers experience specular reflections at the boundaries²¹¹. At zero bias, the distribution of carriers is random and scattered across the left and right side of the structure and no net current flow is observed. Upon applying a bias, carriers gain

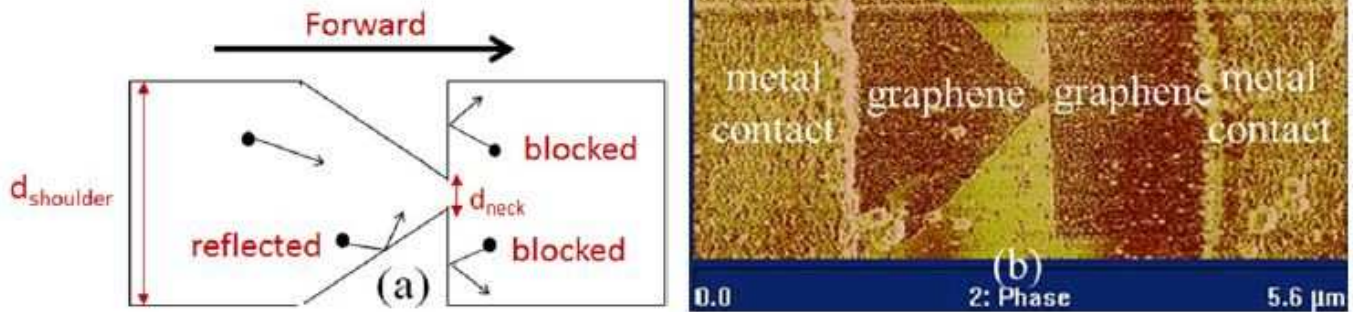


FIG. 28. (a) Schematic of a geometric diode theory of operation. (b) SEM image of a graphene geometric diode with metal contacts developed by Zhu *et al.* (Reprinted from [214], ©IOP Publishing. Reproduced by permission of IOP Publishing. All rights reserved.)

extra velocity in addition to their random thermal drift. For a plain non-constrained geometry, there will be equal net flow from one end to the other, which would define a completely linear I-V characteristic (Ohmic behaviour for perfect conductors). By applying a geometric constraint as the one shown in Figure 28, the motion of the carriers is influenced and favoured in one direction. Carriers moving from the left to right either pass directly through the neck or collide against the angled edge and eventually channel through the neck^{211–214}. On the right hand side, most of the carriers are blocked and reflected away from the neck by the vertical blocks^{211–214}. The probability of electrons passing from the left to the right is enhanced over the probability of them passing from right to left due to the *funnel-like* construction in the forward direction. The neck is required to be of the order of the MFPL, otherwise the probability of electrons passing in reverse direction will increase significantly and compromise the rectification performance.

Neck design is crucial to successful geometric diode performance and is therefore one of the governing factors in the material selection criteria for the device. The material would also have to withstand high current densities through the neck²¹⁴. Metals are suitable to be used¹⁶⁸, however, their MFPL at room temperature is 10–30 nm²¹⁶, which complicates the patterning process and requires expensive techniques such as electron-beam lithography. Graphene has been identified as a suitable and promising alternative to be used in geometric diodes^{210–212,214,215}. Advantages of graphene are that the MFPL can be tailored up to 1 μm ²¹⁷ which means that common lithographic techniques can be used for device patterning and fabrication, resistances are low enough to be matched to the antenna impedance²¹⁴, and very low capacitance values of the order of 1 aF²¹² lead to a low RC time constant of around 1.6 fs²¹¹. All these benefits identify their potential to be used at infrared and even optical frequency rectennas. Recent work on

graphene geometric diodes has shown optical frequency rectification at 10.6 μm wavelength radiation (equivalent to 28 THz) matched with both a metal or a graphene bowtie antenna²¹⁴. Further improvement in the design of these diodes could improve the performance of the device and potentially reach operational frequencies in the visible regime.

VI. RECTENNA DESIGN

Learning from the success in optimising the microwave rectenna, it can be seen that appropriate circuit design is of paramount importance for increasing the performance and efficiency of the device. The solar rectenna is an entirely different challenge as it is constrained by physical limitations and complex material selection criteria and trade-offs. Research is mainly concentrated towards manufacturing and characterisation of antenna and rectifier components, where novel technologies are emerging and great improvement has been seen over the years. Nevertheless, designing the best rectenna architecture is as equally important as optimising its two main constituents. There are many publications on antenna-coupled rectifiers used for optical^{94,172,218–220} or infrared^{108,134,173,176,177,221–223} sensing whereas, to the best of our knowledge, there is no antenna-rectifier device reported to harvest electromagnetic energy at the high solar frequencies. The gap between sensing and harvesting lies in how efficiently the incoming signal is converted and this is what limits the realisation of a true working solar rectenna. We review a few rectenna architectures proposed in the literature, which could result in future success.

Rectennas can either be designed as a planar device or have a geometrical constraint. The diode is used as a passive component with the sole purpose of rectifying the AC signal generated from the antenna. In this case

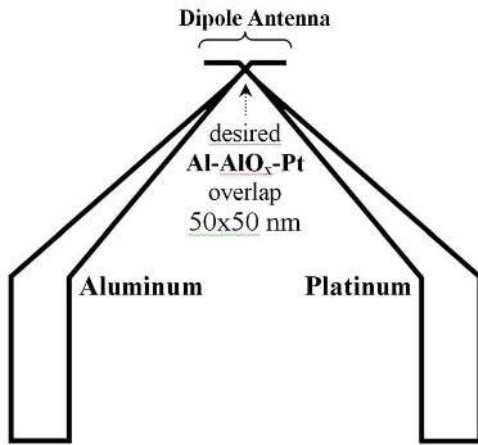
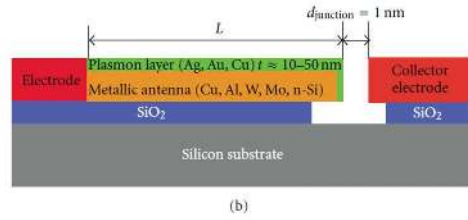
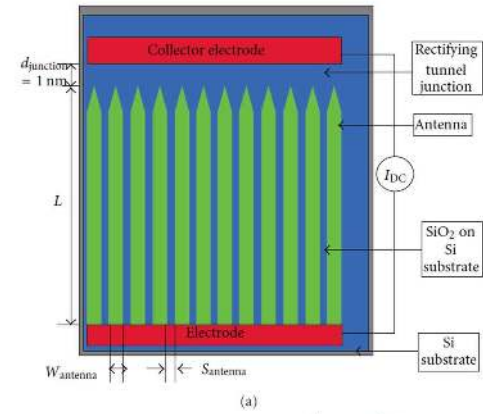


FIG. 29. Schematic diagram of an infrared detector proposed as a suitable design for a solar rectenna. The structure consists of a dipole antenna coupled to a metal-oxide-metal diode. (Reprinted from [173], ©2009 with permission from American Vacuum Society)



(b)

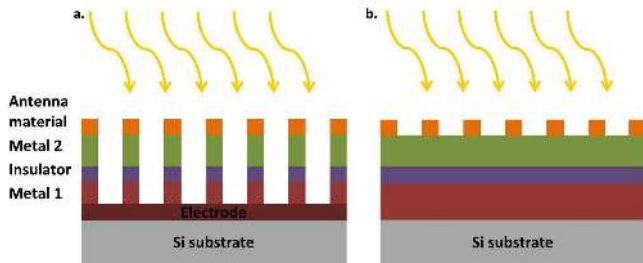
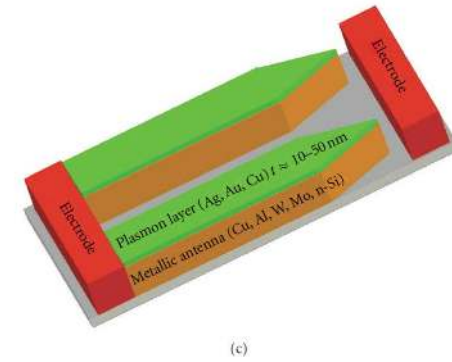


FIG. 30. Schematic diagram of a MIM-based planar-style rectenna architecture with **a.** rectenna array and **b.** antenna array with common rectifier.

the requirements for the diode are emphasised on low resistance and capacitance (resulting in high cut-off frequency), and high I-V asymmetry at a small bias (implying low leakage current and low turn-on voltage). Both planar and geometric designs are suitable for employing this function of the diode. The following three architectures utilise the diodes ability to rectify current.

Figure 29 shows a dipole antenna coupled with a metal-oxide-metal diode based on an Al/AIO_x/Pt structure. This type of architecture is used for IR detection^{134,173,177,221} and up to 28 THz¹⁷⁷ can be sensed with a Ni/NiO/Ni diode. Arrays of the structure can be fabricated either with e-beam lithography or a more economical nanotransfer printing process, which does not compromise the quality of the tunnel junction²²¹. This design gives the benefit of producing small area diodes directly coupled to an antenna, which can be tailored to the length scale of the desired operating frequency. With appropriate material selection and improved impedance match, the cut-off frequency can be increased¹⁷⁷ and electromagnetic energy could potentially be harvested rather



(c)

FIG. 31. Schematic diagram of the rectenna design proposed by Miskovsky *et al.* showing a top **(a)**, side **(b)** and 3D **(c)** view. (Reprinted from [105], ©2012 N.M. Miskovsky *et al.*)

than just detected.

A common approach in rectenna design is a simple planar structure which is composed of antenna-rectifier arrays on a single chip (Figure 30a). The size of the individual Rectennas in the array depends on the aimed harvesting frequency, i.e. for the visible range the rectennas should be of nano-scale dimensions whereas micro-scale would suffice for the near-infrared. Alternatively, the device can be designed as having a common rectifier with an array of antennas (Figure 30b) – bowtie, patch, spiral, etc. The limitations are impedance matching and antenna and rectifier cut-off frequency. With the ever increasing technological advances and device modelling, the necessary goals are seen as realistic and feasible.

Finally, Figure 31 shows schematics of the approach proposed by Miskovsky *et al.*¹⁰⁵. This design consists of an array of needle-like nanostructures, which have been designed to utilise a geometric constraint for the tunnel-

ing mechanism. At the tip of each nanostructure, a 1 nm junction is formed which can either form a MVM-type barrier or if an insulator is placed then the barrier will be an MIM-type. The fabrication of this type of structure is very complex, but was recently optimised by use of selective area atomic layer deposition – a technique developed and patented by Prof. Brian Willis of the University of Connecticut¹⁹⁷. Similar design can be implemented with the described Graphene geometric diode²¹⁴ where instead of leaving a tunnel junction, the tip of the needle-like nanostructure is brought close to the collector electrode. This rectenna design is very promising and yet to be optimised in terms of material selection, ease of manufacturing and reliability.

Another planar device design has already been introduced in Section V.A, whereby the rectifier is employed as an active component producing a current enhancement as a result of hot electron injection into the metal and crossing over a Schottky barrier, which is seen as a reverse current enhancement in an I-V plot (similar to what is observed during the photovoltaic effect). The design necessitates a diode with low barrier height, low leakage current and a suitable top metal to increase the amount of electrons excited to a higher energy state. It must be made clear that this device, although having components similar to a rectenna, is fundamentally different to the rectenna. With rectennas, the aim is to optimise the absorption by a load, whereas for hot-electron devices it is in optimising the absorption efficiency of the LSPR nanoparticle. A good review of hot-electron devices can be found in [224]. Efficiency estimates for rectennas prevail to those for hot-electron devices, although this remains an intriguing field for future development.

VII. SOCIO-ECONOMIC IMPACT & FUTURE WORK

The defining milestone for the rectenna was the Raytheon development of the microwave rectenna in the 1960s¹³. The ability to capture background radiation to demonstrate a working device, a helicopter no less, was a remarkable achievement. Concerns regarding energy security have led to a growing interest in harvesting solar radiation – a huge source of energy offering roughly 350 W/m^2 . In 2011, the International Energy Agency predicted that solar energy technologies such as photovoltaic panels, solar water heaters and power stations built with solar collector mirrors could provide a third of the world’s energy by 2060. Unsurprisingly, there was no mention of a rectenna device because there has never been a successful demonstration of a solar rectenna with even modest efficiencies of a few percent.

Solar cells made of silicon have already made a huge impact in a whole range of devices that use Si cells for power and they have also made a tremendous socio-economic impact in developing countries. It is worth recalling that around 1.2 billion people on our planet

have no access to power and about 2.8 billion people use solid fuels (wood, charcoal, coal and dung) for cooking and heating²²⁵. Every year fumes and smoke from open cooking fires kill approximately 1.5 million people mostly women and children, from emphysema and other respiratory diseases and therefore a key responsibility for scientists and engineers is to carry out research to address such inequality. The advent of “plastic electronics” offers the possibility of inexpensive, flexible solar cells using semiconductors albeit at lower efficiencies of around 5-10%.

The rectenna is simply another means of collecting background radiation whether it be at optical frequencies in the solar spectrum (430-790 THz) or at IR frequencies (0.3-430 THz) meaning that cells could operate at night. The ultimate goal then of a rectenna is to augment current technologies and with current low frequency efficiencies of over 90%, the incentive to carry out research is obvious. However, the situation is not so simple and the key observation is that as the frequency of operation of the rectenna rises, the efficiency drops so that at solar frequencies most predicted efficiencies are a fraction of one percent. Here then is the first research challenge: to increase the efficiency to match at least the photovoltaic efficiencies offered by low cost plastic electronic solar PV (5-10%). Second, a rectenna device capable of operation at solar frequencies, which is a tremendous fabrication challenge with diodes of nanometre dimensions needed. Using expensive e-beam lithography techniques may demonstrate proof of principle but are too costly for commercialisation. Therefore, the engineering challenge is to find inexpensive fabrication techniques capable of scale-up and able to provide the efficiencies required.

So what are the prospects? There is little doubt that the task is hard – low cost fabrication of nano antennas and diodes of nm dimensions is non-trivial. But the rewards are significant. Perhaps most important is that, as noted in Section III, there is no scientific reason suggesting that a rectenna device operating at solar frequencies should not be capable of efficiencies in the region of 10% and ideally far greater. This then is the challenge and the potential reward is reason alone why there are several laboratories exploring such technologies. Let us be bold and assume success in this goal. What would be the implications? First of all, to have developed the technologies to fabricate the nanoantennas and diodes using scalable manufacturing processes would provide an extra option to the generation of energy. Second, success would not only impact upon a wide range of energy technologies but would be transferable such that it would also transform wide range of technologies associated with for example the Health, Transport and Infrastructure sectors. These sectors are fundamental to our socio-economic progress.

This review has identified many positive points on the development of the solar rectenna. Modelling the conversion efficiency has been attempted on many occasions, however as seen in Figure 8 the many different assumptions predict a wide spread of efficiency values. The sci-

entific community understands the operational theory of the device but further work is required to confirm and identify the major contributing loss and gain effects in order to accurately predict the efficiency. There is also lack of experimentally derived efficiency results at the high solar frequencies as research was until now mainly concentrated on developing new technology for nanofabrication and optimisation of antennas and diodes, modelling device response and theoretically estimating matching suitability. In the course of this review, new developments have been highlighted, which have given promising results for both the antenna and the rectifier. The technology is mature enough for it to be used to fabricate and characterise prototype rectenna devices. Testing prototypes will help identify further work, which needs to be carried out on the antenna and rectifier. A very useful methodology has been developed to characterise materials for MIM diodes and some experimental results of actual devices have been reported, identifying potential diodes which could be branded with having ideal I-V characteristics and far exceed the minimum figure of merit requirements. However, these diodes need to be characterised for their cut-off frequency and matching with an antenna. Work on the other rectifiers (MIIM and geometric diodes) is yet too undeveloped to have conclusive results, but provisional tests show great potential and they must be pursued and optimised.

In summary, despite the fact that Tesla suggested the transference of energy through electromagnetic radiation in the 1890s and despite the practical development of rectennas in the 1960-70s, the goal of solar rectification, or even large transfers of high-frequency power, has not yet been realised at the efficiencies we need. The two key issues that we need to address are to increase the efficiencies to useable levels, here suggested at 5-10%, and to develop low cost scalable manufacturing routes. The secondary goal is to increase the efficiency and here we can only speculate but we should harbour an ambition to obtain efficiencies exceeding that of the best solar cells tested to date of around 45%²²⁶.

VIII. SUMMARY

In this article, the history and operation of the rectenna device have been reviewed from its initial concept as a receiver in microwave power transmission through to developments in pursuit of high-efficiency solar harvesting. Rectennas have been studied exten-

sively for application in wireless energy transmission by use of man-made microwave energy with conversion efficiencies as high as 92%, which brings optimism to the goal of beating the Shockley-Queisser limit by achieving high-efficiency solar rectenna energy converters. Efficiency trends have been reviewed, where experimentally obtained efficiency values for rectenna devices have shown an overall decrease with an increase in operating frequency. Although there is no agreement on an optimised model for characterising the performance of a rectenna, all theoretical work suggests that to improve efficiency, three criteria must be met – 1) efficient absorption by the antenna at the desired frequency, 2) a high cut-off frequency diode to efficiently rectify the incoming signal and 3) impedance matching between antenna and rectifier to avoid signal transfer losses. Solving these three challenges would result in efficient device operation, which has the potential of operating at higher thermodynamic efficiency than current photovoltaic cells. Work on improving the performance of the antenna and rectifier has been reviewed showing substantial technological advancement and improved theoretical understanding of these two device components. Rectenna design also plays a major role in optimising the device and a few architectures have been discussed for their suitability. It was finally argued that the most essential future work required is to build rectenna devices based on optimised technology and design, as this is currently lacking in the literature. Attempts have been made on antenna-rectifier devices which have been aimed to work as IR or visible light sensors. Fabricating rectenna prototypes will enable scientists to characterise and assess their performance, giving them opportunity to identify new areas for necessary optimisation.

ACKNOWLEDGMENTS

This work was supported in part by EPSRC grant number EP/G060940/1. Peter Gammon would like to gratefully acknowledge the financial support from the Royal Academy of Engineering. J. S. Pang and P. K. Petrov acknowledge the financial support under the King Abdullah University for Science and Technology (KAUST) Global Collaborative Research Academic Excellence Alliance (AEA) and Academic Partnership Programs (APP).

-
- [1] W. Shockley & H.J. Quieser: Detailed balance limit of efficiency of p-n junction solar cells, *Journal of Applied Physics* **32**(3), p. 510-519 (1961)
 - [2] C.H. Henry: Limiting efficiencies of ideal single and multiple energy gap terrestrial solar cells, *Journal of Applied Physics* **51**, p. 4494-4500 (1980)
 - [3] R. Corkish, M.A. Green & T. Puzzer: Solar energy collection by antennas, *Solar Energy* **73**(6), p. 395-401 (2002)
 - [4] D.Y. Goswami, S. Vijayaraghavan, S. Lu & G. Tamm: New and emerging developments in solar energy, *Solar Energy* **76**, p. 33-43 (2004)

- [5] B. Berland: Photovoltaic Technologies Beyond the Horizon: Optical Rectenna Solar Cell, Subcontractor Report, National Renewable Energy Laboratory, (2002), Found online at: <http://www.nrel.gov/docs/fy03osti/33263.pdf>
- [6] J.O. McSpadden, L. Fan & K. Chang: Design and Experiments of a High-Conversion-Efficiency 5.8-GHz Rectenna, *IEEE Trans. Microwave Theory Tech.* **46**(12), p. 2053-2060 (1998)
- [7] J.J. Nahas: Modeling and Computer Simulation of a Microwave-to-DC Energy Conversion Element, *IEEE Trans. Microwave Theory Tech.* **23**12, p. 1030-1035 (1975)
- [8] T. Razban, M. Bouthinon & A. Coumes: Microstrip circuit for converting microwave low power to DC energy, *IEE Proceedings* **132**(2), p.107-109 (1985)
- [9] V. Mlinar: Engineered nanomaterials for solar energy conversion, *Nanotechnology* **24**, 042001 (2013)
- [10] R.L. Bailey: A proposed new concept for a solar-energy converter, *Journal of Engineering for Power* **94**, p. 73-77 (1972)
- [11] J.D. Kraus: *Antennas, 2nd ed*, McGraw-Hill, New York 1988
- [12] H. Hertz: *Dictionary of Scientific Biography vol. VI*, New York: Scribner, p. 340-349
- [13] W.C. Brown: The History of Power Transmission by Radio Waves, *IEEE Trans. Microwave Theory Tech.* **32**(9), p. 1230-1242 (1984)
- [14] E.C. Okress, Ed.: *Microwave Power Engineering vols. I, II*, New York: Academic, 1968
- [15] R.H. George: Solid state power rectifications, (in *Okress, Microwave Power Engineering vol. I*, New York: Academic, 1968), p. 275-294
- [16] W.C. Brown, R.H. George, N.I. Heenan & R.C. Wonson: Microwave to dc converter, U.S. Patent 3434678, March 26, 1969
- [17] W.C. Brown: The Microwave Powered Helicopter, *J. Microwave Power* **1**(1) (Symposium on Microwave Power, University of Alberta, March 24th, 1966)
- [18] P.E. Glaser: Power from the sun, Its future, *Science* **162**, p. 857-886 (1968)
- [19] W.C. Brown: Satellite solar power station and microwave transmission to earth, *J. Microwave Power* **5**(4) (1970)
- [20] W.C. Brown & O.E. Maynard: Microwave power transmission in the satellite solar power station system, Raytheon Report ER 72-4038, 27 January 1972
- [21] W.C. Brown: Satellite power stations - A new source of energy?, *IEEE Spectrum* **10**(3), p.38-47 (1973)
- [22] P.E. Glaser, O.E. Maynard, J. Macfcovciak Jr. & E.L. Ralph: Feasibility study of a satellite solar power station, NASA Lewis Research Center, Cleveland, OH, CR-2357, NTIS N74-17784, 1974
- [23] P.E. Glaser: Method and apparatus for converting solar radiation to electrical power, U.S. Patent 3 781 647, 1973
- [24] N. Shimokura, N. Kaya, N. Shinohara & H. Matsumoto: Point-to-point microwave power transmission experiment, *Trans. Inst. Elect. Eng. Jpn. B* **116**(6), p. 648-653 (1996)
- [25] N. Shinohara & H. Matsumoto: Experimental study of large rectenna array for microwave energy transmission, *IEEE Trans. Microwave Theory Tech.* **46**(3), p.261-268 (1998)
- [26] P.E. Glaser: An Overview of the Solar Power Satellite Option, *IEEE Trans. Microwave Theory Tech.* **40**(6), p. 1230-1238 (1992)
- [27] J.O. McSpadden, F.E. Little, M.B. Duke & A. Ignatiev: An in-space wireless energy transmission experiment, *Proc. IECEC Energy Conversion Engineering Conf.* **1**, p. 468-473 (1996)
- [28] T. Yoo & K. Chang: Theoretical and experimental development of 10 and 35 GHz rectennas, *IEEE Trans. Microwave Theory Tech.* **40**, p. 1259-1266 (1992)
- [29] L.W. Epp, A.R. Khan, H.K. Smith & R.P. Smith: A compact dual-polarized 8.51-GHz rectenna for high-voltage (50 V) Actuator applications, *IEEE Trans. Microwave Theory Tech.* **48**, p. 111-120 (2000)
- [30] Y. Fujino, T. Ito, M. Fujita, N. Kaya, H. Matsumoto, K. Kawabata, H. Sawada & T. Onodera: A driving test of a small DC motor with a rectenna array, *IEICE Trans. Commun.* **E77-B**(4), p. 526-528 (1994)
- [31] J.A. Hagerty, F.B. Helmbrecht, W.H. McCalpin, R. Zane & Z.B. Popović: Recycling Ambient Microwave Energy With Broad-Band Rectenna Arrays, *IEEE Trans. Microwave Theory Tech.* **52**(3), p.1014-1024 (2004)
- [32] X. Yang, C. Jiang, A.Z. Elsherbeni, F. Yang & Y.Q. Wang: A Novel Compact Printed Rectenna for Data Communication Systems, *IEEE Trans. Anten. Prop.* **61**(5), p. 2532-2539 (2013)
- [33] J.C. Fletcher & R.L. Bailey: Electromagnetic wave energy Converter, U.S. Patent 3 760 257, 1973
- [34] R.L. Bailey, P.D. Callahan & M. Zahn: Electromagnetic Wave Energy Conversion Research, Final Report April-30 September, NASA-CR-145876, 1975
- [35] A.M. Marks: Device for conversion of light power to electric power, U.S. Patent 4 445 050, 1984
- [36] A.M. Marks: Ordered dipolar light-electric power converter, U.S. Patent 4 574 161, 1986
- [37] A.M. Marks: Femto diode and applications, U.S. Patent 4 720 642, 1988
- [38] A.M. Marks: Lighting device with quantum electric/light power converters, U.S. Patent 4 972 094, 1990
- [39] G.H. Lin, R. Abdu & J.O.M. Bockris: Investigation of resonance light absorption and rectification by sub-nanostructures, *J. Appl. Phys.* **80**, p.565-568 (1996)
- [40] T.K. Gustafson & K. Billman: Metal-oxide-metal optical diodes, Ames R.C. Rsch. Review, NASA J. p. 205-208 (1974)
- [41] B. Strassner & K. Chang: Microwave Power Transmission: Historical Milestones and System Components, *Proc. of the IEEE* **101**(6), p. 1379-1395 (2013)
- [42] R.M. Dickinson & W.C. Brown: Radiated microwave power transmission system efficiency measurements, Jet Propulsion Lab., California Inst. Technol. Pasadena, CA, USA, Tech. Memo 33-727, Mar. 15, 1975
- [43] A.A. Konovaltsev, Y.A. Luchaninov, M.A. Omarov & V.M. Shokalo: Developing Wireless Energy Transfer Systems Using Microwave Beams: Applications and Prospects, *Telecom. and Radio Eng.* **55**(2), p. 21-29 (2001)
- [44] J.O. McSpadden, T.W. Yoo & K. Chang: Theoretical and Experimental Investigation of a Rectenna Element for Microwave Power Transmission, *IEEE Trans. Microwave Theory Tech.* **40**(12), p. 2359-2366 (1992)
- [45] W.C. Brown & J.F. Triner: Experimental Thin-Film, Etched-Circuit Rectenna, *Microwave Symposium, IEEE*

- MTT-S Digest K-4*, p. 185-187 (1982)
- [46] J. Zbitou, M. Latrach & S. Toutain: Hybrid Rectenna and Monolithic Integrated Zero-Bias Microwave Rectifier, *IEEE Trans. Microwave Theory Tech.* **54**(1), p. 147-152 (2006)
- [47] H. Takhedmit, L. Cirio, S. Bellal, D. Delcroix & O. Picon: Compact and Efficient 2.45 GHz Circularly Polarised Shorted Ring-slot Rectenna, *Electronic Letters* **48**(5), (2012)
- [48] H. Sun, Y.-X. Guo & Z. Zhong: A high-sensitivity 2.45 GHz rectenna for low input power energy harvesting, *IEEE Antennas and Propagation Society International Symposium (APSURSI)*, (2012)
- [49] H. Sun, Y.-X. Guo, M. He & Z. Zhong: Design of a High-Efficiency 2.45-GHz Rectenna for Low-Input-Power Energy Harvesting, *IEEE Antennas and Wireless Propagation Letters* **11**, p. 929-932 (2012)
- [50] W.C. Brown & C.K. Kim: Recent Progress in Power Reception Efficiency in a Free-Space Microwave Power Transmission System, *Microwave Symposium Digest* **74**(1), p. 332-333 (1974)
- [51] R.J. Gutmann & J.M. Borrego: Power Combining in an Array of Microwave Power Rectifiers, *IEEE Trans. Microwave Theory Tech.* **27**(12), p. 958-968 (1979)
- [52] F.-J. Huang, C.-M. Lee, C.-L. Chang, L.-K. Chen, T.-C. Yo & C.-H. Luo: Rectenna Application of Miniaturized Implantable Antenna Design for Triple-Band Biotelemetry Communication, *IEEE Trans. Antennas Prop.* **59**(7), p. 2646-2643 (2011)
- [53] J. Heikkinen & M. Kivikoski: A Novel Dual-Frequency Circularly Polarized Rectenna, *IEEE Antennas and Wireless Propagation Letters* **2**, p. 330-333 (2003)
- [54] Y.-H. Suh & K. Chang: A High-Efficiency Dual-Frequency Rectenna for 2.45- and 5.8-GHz Wireless Power Transmission, *IEEE Trans. Microwave Theory Tech.* **50**(7), p. 1784-1789 (2002)
- [55] Y.-J. Ren, M.F. Farooqui & K. Chang: A Compact Dual-Frequency Rectifying Antenna with High-Orders Harmonic Rejection, *IEEE Trans. Antennas Prop.* **55**(7), p. 2110-2113 (2007)
- [56] T. Ito, Y. Fujino & M. Fujita: Fundamental experiment of a rectenna array for microwave power reception, *IEICE Trans. Commun.* **E76-B**(12), p. 1508-1513 (1993)
- [57] J.-Y. Park, S.-M. Han & T. Itoh: A Rectenna Design With Harmonic-Rejecting Circular-Sector Antenna, *IEEE Antennas and Wireless Propagation Letters* **3**, p. 52-54 (2004)
- [58] Y.-Y. Gao, X.-X. Yang, C. Jiang & J.-Y. Zhou: A Circularly Polarized Rectenna with Low Profile for Wireless Power Transmission, *Progress in Electromagnetics Research Letters* **13**, p. 41-49 (2010)
- [59] J.O. McSpadden, L. Fan & K. Chang: A High-Conversion-Efficiency 5.8-GHz Rectenna, *Microwave Symposium, IEEE MTT-S Digest* **WE2B-6**, p. 547-550 (1997)
- [60] S.S. Bharj, R. Camisa, S. Grober, F. Wozniak & E. Pendleton: High Efficiency C-Band 1000 Element Rectenna Array For Microwave Powered Application, *Microwave Symposium, IEEE MTT-S Digest* **IF1 G-1**, p. 301-303 (1992)
- [61] Y. Suh, C. Wang & K. Chang: Circularly Polarised Truncated-Corner Square Patch Microstrip Rectenna for Wireless Power Transmission, *Electronic Letters* **36**(7), p.600-602 (2000)
- [62] B. Strassner & K. Chang: Highly Efficient C-Band Circularly Polarized Rectifying Antenna Array for Wireless Microwave Power Transmission, *IEEE Trans. Antennas Prop.* **51**(6), p. 1347-1356 (2003)
- [63] B. Strassner & K. Chang: A circularly polarized rectifying antenna array for wireless microwave power transmission with over 78% efficiency, *IEEE MTT-S Int. Microwave Symp. Dig.*, p. 1535 -1538 (2002)
- [64] M. Ali, G. Yang & R. Dougal: A New Circularly Polarized Rectenna for Wireless Power Transmission and Data Communication, *IEEE Antennas and Wireless Propagation Letters* **4**, p. 205-208 (2005)
- [65] M. Ali, G. Yang & R. Dougal: Miniature Circularly Polarized Rectenna with Reduced Out-of-Band Harmonics, *IEEE Antennas and Wireless Propagation Letters* **5**, p. 107-110 (2006)
- [66] Y.-J. Ren & K. Chang: 5.8 GHz Broadened Beam-width Rectifying Antennas Using Non-uniform Antenna Arrays, *IEEE Antennas and Propagation Society International Symposium*, p. 867-870 (2006)
- [67] X.-X. Yang, C. Jiang, A.Z. Elsherbeni, F. Yang & Y.-Q. Wang: A Novel Compact Printed Rectenna for Communication Systems, Power and Energy Engineering Conference (APPEEC) (2012)
- [68] K. Fujimori, K. Tada, Y. Ueda, M. Sanagi & S. Nogi: Development of High Efficiency Rectification Circuit for mW-class Rectenna, *IEEE European Microwave Conference* **2** (2005)
- [69] B. Strassner & K. Chang: 5.8-GHz Circularly Polarized Dual-Rhombic-Loop Traveling-Wave Rectifying Antenna for Low Power-Density Wireless Power Transmission Application, *IEEE Trans. Microwave Theory Tech.* **51**(5), p. 1548-1553 (2003)
- [70] C.K. Chin, Q. Xue & C.H. Chan: Design of a 5.8-GHz Rectenna Incorporating a New Patch Antenna, *IEEE Antennas and Wireless Propagation Letters* **4**, p. 175-178 (2005)
- [71] Y.-J. Ren & K. Chang: 5.8-GHz Circularly Polarized Dual-Diode Rectenna and Rectenna Array for Microwave Power Transmission, *IEEE Trans. Microwave Theory Tech.* **54**(4), p. 1495-1502 (2006)
- [72] W.-H. Tu, S.-H. Hsu & K. Chang: Compact 5.8-GHz Rectenna Using Stepped-Impedance Dipole Antenna, *IEEE Antennas and Wireless Propagation Letters* **6**, p. 282-284 (2007)
- [73] Y. Xuexia, X. Junshu, X. Deming & X. Changlong: X-Band Circularly Polarized Rectennas for Microwave Power Transmission Applications, *J. of Electronics (China)* **25**(3), p. 389-393 (2008)
- [74] G. Monti, L. Tarricone & M. Spartano: X-Band Planar Rectenna, *IEEE Antennas and Wireless Propagation Letters* **10**, p. 1116-1119 (2010)
- [75] T.-W. Yoo & K. Chang: 35 GHz Integrated Circuit Rectifying Antenna with 33% Efficiency, *Electronic Letters* **27**(23), p. 2117 (1991)
- [76] D. Hong-Lei & K. Li: A Novel High-Efficiency Rectenna for 35GHz Wireless Power Transmission, *4th Int. Conf. Micr. Mill. Wave Tech. Proc.*, p. 114-117 (2004)
- [77] H.-K. Chiou & I.-S. Chen: High-Efficiency Dual-Band On-Chip Rectenna for 35- and 94- GHz Wireless Power Transmission in 0.13- μ m CMOS Technology, *IEEE Trans. Microwave Theory Tech.* **58**(12), p. 3598-3606 (2010)

- [78] Y. Pinhasi, I.M. Yakover, A.L. Eichenbaum & A. Gover: Efficient Electrostatic-Accelerator Free-Electron Masers for Atmospheric Power Beaming, *IEEE Trans. Plasma Science* **24**(3), p. 1050-1057 (1996)
- [79] P. Koert & J.-T. Cha: Millimeter Wave Technology for Space Power Beaming, *IEEE Trans. Microwave Theory Tech.* **40**(6), p. 1251-1258 (1992)
- [80] Y.-J. Ren, M.-Y. Li & K. Chang: 35 GHz rectifying antenna for wireless power transmission, *Electronic Letters* **43**(11), (2007)
- [81] P. Koert, J.-T. Cha & M. Macina: 35 and 94 GHz Rectifying Antenna Systems, (Power from Space Dig., Paris, France, Aug. 1991), p. 541-547
- [82] W.C. Brown: Optimization of the Efficiency and other Properties of the Rectenna Element, *Microwave Symposium, IEEE MTT-S International*, p. 142-144 (1976)
- [83] W.C. Brown: Experiments Involving A Microwave Beam to Power and Position a Helicopter, *IEEE Trans. Aerospace and Electronics Sys.* **AES-5**(5), p. 692-702 (1969)
- [84] R. Corkish, M.A. Green, T. Puzzer & T. Humphrey: Efficiency of antenna solar collection, *Proc. Photovoltaic Energy Conversion* **3**, p. 2682-2685 (2003)
- [85] NIST: Optical Nanoantennas and Nanodiodes using Atomic Layer Deposition, (2002), found online: www.boulder.nist.gov/div814/nanotech/antennas
- [86] C. Balanis, *Antenna Theory. Analysis and Design 2nd Ed.*, Wiley, New York, 1997
- [87] J.M. Nunzi: Requirements for a rectifying antenna solar cell technology, *Proc. of SPIE* **7712**, (2010)
- [88] B. Berland, L. Simpson, G. Nuebel, T. Collins & B. Lanning: Optical rectenna for direct conversion of sunlight to electricity, (National Center for Photovoltaics Program Review Meeting, NREL, 2001), p. 323-324
- [89] H. Mashaal & J.M. Gordon: Efficiency limits for the rectification of solar radiation, *J. Appl. Phys.* **113**, 193509 (2013)
- [90] S. Joshi & G. Moddel: Efficiency limits of rectenna solar cells: Theory of broadband photon-assisted tunneling, *Applied Physics Letters* **102**, 083901 (2013)
- [91] D.K. Kotter, S.D. Novak, W.D. Slafer & P. Pinhero: Solar nantenna electromagnetic collectors, (2nd International Conference on Energy Sustainability, August 2008), p. 10-14
- [92] E. Briones, J. Alda & F.J. Gonzlez: Conversion Efficiency of Broad-Band Rectennas for Solar Energy Harvesting Applications, *Optics Express* **21**(S3), p. A412-A418 (2013)
- [93] P.B. Lerner, N.M. Miskovsky, P.H. Cutler, A. Mayer & M.S. Chung: Thermodynamic analysis of high frequency rectifying devices: Determination of the efficiency and other performance parameters, *Nano Energy* **2**, p. 368-376 (2013)
- [94] M.W. Knight, H. Sobhani, P. Nordlander & N.J. Halas: Photodetection with Active Optical Antennas, *Science* **332**, p. 702-704 (2011)
- [95] Z. Ma & G.A.E. Vandenbosch: Optimal Solar energy harvesting efficiency of nano-rectenna systems, *Solar Energy* **88**, p. 163-174 (2013)
- [96] M. Sarehraz, K. Buckle, T. Weller, E. Stefanakos, S. Bhansali, Y. Goswami & S. Krishnan: Rectenna Developments for Solar Energy Collection, (Photovoltaic Specialists Conference, 2005), p. 78-81
- [97] G.A.E. Vandenbosch & Z. Ma: Upper bounds for the solar energy harvesting efficiency of nano-antennas, *Nano Energy* **1**, p. 494-502 (2012)
- [98] E. Stefanakos, Y. Goswami & S. Bhansali: Rectenna Solar Energy Harvester, US Patent 8 115 683, B1, 2012
- [99] G. Moddel & S. Grover, editors: *Rectenna Solar Cells*, Springer, New York, 2013
- [100] Z. Zhu, S. Joshi, B. Pelz & G. Moddel: Overview of optical rectennas for solar energy harvesting, *Proc. of SPIE* **8824**, 882400 (2013)
- [101] I. Brinster, J. Lohn & D. Linden: An evolved rectenna for sensor networks, *IEEE APSURSI*, p. 418-419 (2013)
- [102] P.T. Landsberg & G. Tonge: Thermodynamics of the conversion of diluted radiation, *J. Phys. A: Math. Gen.* **12**(4), p. 551-561, (1979)
- [103] E. Giovine, R. Casini, D. Dominijanni, A. Notargiacomo, M. Ortolani & V. Foglietti: Fabrication of Schottky diodes for terahertz imaging, *Microelectronic Engineering* **88**, p. 2544-2546 (2011)
- [104] A. Sanchez, C.F. Davis Jr, K.C. Liu & A. Javan: The MOM Tunneling Diode: Theoretical Estimate of its Performance at Microwave and Infra Frequencies, *J. Appl. Phys.* **49**, p. 5270-5277 (1978)
- [105] N.M. Miskovsky, P.H. Cutler, A. Mayer, B.L. Weiss, B. Willis, T.E. Sullivan & P.B. Lerner: Nanoscale Devices for Rectification of High Frequency Radiation from the Infrared through the Visible: A New Approach, *J. Nanotechnology*, (2012)
- [106] L. Brillouin: Can the Rectifier Become a Thermodynamical Demon?, *Phys. Rev.* **78**, p. 627 (1950)
- [107] J.B. Andersen & A. Frandsen: Absorption Efficiency of Receiving Antennas, *IEEE Trans. Antennas Prop.* **53**(9), p. 2843-2849 (2005)
- [108] C. Fumeaux, W. Herrmann, F.K. Kneubühl & H. Rothuizen: Nanometer thin-film Ni-NiO-Ni diodes for detection and mixing of 30THz radiation, *Infrared Physics & Technology* **39**, p. 123-183 (1998)
- [109] C. Fumeaux, J. Alda & G. D. Boreman: Lithographic antennas at visible frequencies, *Opt. Lett.* **24**, p. 1629 (1999)
- [110] F. J. González & G. D. Boreman: Comparison of dipole, bowtie, spiral and log-periodic IR antennas, *Infrared Phys. & Technol.* **46**, p. 418-428 (2005)
- [111] S. Krishnan, H. La Rosa, E. Stefanakos, S. Bhansali & K. Buckle: Design and development of batch fabricatable metal-insulator-metal diode and microstrip slot antenna as rectenna elements, *Sensors and Actuators A* **142**, p. 40-47 (2008)
- [112] Y.-J. Ren & K. Chang: New 5.8-GHz circularly polarized retrodirective rectenna arrays for wireless power transmission, *IEEE Trans. Microwave Theory Tech.* **54**, p. 2970-2976 (2006)
- [113] R. P. Feynman: There's plenty of room at the bottom, *Eng. Sci.* **23**, p. 22-36 (1960)
- [114] P. Muhlschlegel: Resonant Optical Antennas, *Science* **308**, p.1607-1609 (2005)
- [115] B. Hecht, P. Muhlschlegel, J. N. Farahani, H.-J. Eisler & D. W. Pohl: Chapter 9 – Resonant optical antennas and single emitters, *Tip Enhancement*, Elsevier: Amsterdam, p. 275-307 (2007)
- [116] P. Biagioni, J.-S. Huang & B. Hecht: Nanoantennas for visible and infrared radiation, *Reports Prog. Phys.* **75**, 024402 (2012)

- [117] J. D. Jackson: *Classical Electrodynamics, 3rd ed.*, John Wiley & Sons, 1998
- [118] S. A. Maier: *Plasmonics: Fundamentals and Applications*, Springer, 2007
- [119] U. Kreibig & M. Vollmer: *Optical properties of metal clusters*, Springer, 1995
- [120] A. D. Rakic, A. B. Djurišić, J.M. Elazar & M. L. Majewski: Optical Properties of Metallic Films for Vertical-Cavity Optoelectronic Devices, *Appl. Opt.* **37**, p. 5271 (1998)
- [121] C. F. Bohren & D. R. Huffman: *Absorption and Scattering of Light by Small Particles*, Wiley, 2008
- [122] A. Centeno, F. Xie, J. Breeze & N. Alford: Calculations of scattering and absorption efficiencies of noble metal nanoparticles, (Applied Electromagnetics Conference (AEMC), IEEE, 2011), p. 1-4
- [123] B. T. Draine & P. J. Flatau: Discrete-dipole approximation for scattering calculations, *J. Opt. Soc. Am.* **11**, p. 1491 (1994)
- [124] C. G. Khoury, S. J. Norton & T. Vo-Dinh: Plasmonics of 3-D nanoshell dimmers using multipole expansion and finite element method, *ACS Nano* **3**(9), p. 2776-2788 (2009)
- [125] A. F. Oskooi, D. Roundy, M. Ibanescu, P. Bermel, J. D. Joannopoulos & S. G. Johnson: Meep: A Flexible free-software package for electromagnetic simulations by the FDTD method, *Comput. Phys. Commun.* **181**, p. 687-702 (2010)
- [126] A. Centeno, N. Alford & F. Xie: Predicting the fluorescent enhancement rate by gold and silver nanospheres using finite-difference time-domain analysis, *IET Nanobiotechnology* **7**, p. 50-58 (2010)
- [127] A. Centeno, B. Ahmed, H. Reehal & F. Xie: Diffuse scattering from hemispherical nanoparticles at the air-silicon interface, *Nanotechnology* **24**, 415402 (2013)
- [128] Z. Fang, Z. Liu, Y. Wang, P. M. Ajayan, P. Nordlander & N. J. Halas: Graphene-Antenna Sandwich Photodetector, *Nano Lett.* **12**, p. 3808-3813 (2012)
- [129] I. Goykhman, B. Desiatov, J. Khurgin, J. Shappir & U. Levy: Locally Oxidized Silicon Surface-Plasmon Schottky Detector for Telecom Regime, *Nano Lett.* **11**, p. 2219-2224 (2011)
- [130] S. Mukherjee, F. Libisch, N. Large, O. Neumann, L.V. Brown, J. Cheng, J. B. Lassiter, E. A. Carter, P. Nordlander & N.J. Halas: Hot Electrons Do the Impossible: Plasmon-Induced Dissociation of H₂ on Au, *Nano Lett.* **13**, p. 240-247 (2013)
- [131] F. Wang & N. A. Melosh: Plasmonic Energy Collection through Hot Carrier Extraction, *Nano Lett.* **11**, p. 5426-5430 (2011)
- [132] F. Xie, J. S. Pang, A. Centeno, M. P. Ryan, D. J. Riley & N.M. Alford: Nanoscale control of Ag nanostructures for plasmonic fluorescence enhancement of near-infrared dyes, *Nano Res.* **6**, p. 496-510 (2013)
- [133] A. Bonakdar, J. Kohoutek, D. Dey & H. Mohseni: Optomechanical nanoantenna, *Opt. Lett.* **37**, p. 3258 (2012)
- [134] S. Grover, O. Dmitriyeva, M.J. Estes & G. Model: Travelling-Wave Metal/Insulator/Metal Diodes for Improved Infrared Bandwidth and Efficiency of Antenna-Coupled Rectifiers, *IEEE Trans. Nanotech.* **9**(6), p. 716-722 (2010)
- [135] E. C. Kinzel, R. L. Brown, J. C. Ginn, B. A. Lail, B. A. Slovick & G. D. Boreman: Design of an MOM diode-coupled frequency-selective surface, *Microw. Opt. Technol. Lett.* **55**, p. 489-493 (2013)
- [136] J. C. Reed, H. Zhu, A. Y. Zhu, C. Li & E. Cubukcu: Graphene-Enabled Silver Nanoantenna Sensors, *Nano Lett.* **12**, p. 4090-4094 (2012)
- [137] Z. Fang, S. Thongrattanasiri, A. Schlather, Z. Liu, L. Ma, Y. Wang, P. M. Ajayan, P. Nordlander, N. J. Halas & F. J. G. de Abajo: Gated Tunability and Hybridization of Localized Plasmons in Nanostructured Graphene, *ACS Nano* **7**, p. 2388-2395 (2013)
- [138] J.-J. Greffet, M. Laroche & F. Marquier: Impedance of a Nanoantenna and a Single Quantum Emitter, *Phys. Rev. Lett.* **105** (2010)
- [139] N. Liu, F. Wen, Y. Zhao, Y. Wang, P. Nordlander, N. J. Halas & A. Alù: Individual Nanoantennas Loaded with Three-Dimensional Optical Nanocircuits, *Nano Lett.* **13**, p. 142-147 (2013)
- [140] L. J. Guo: Nanoimprint Lithography Methods and Material Requirements, *Adv. Mater.* **19**, p. 495-513 (2007)
- [141] I. Bergmair, B. Dastmalchi, M. Bergmair, A. Saeed, W. Hilber, G. Hesser, C. Helgert, E. Pshenay-Severin, T. Pertsch, E. B. Kley, U. Hübner, N. H. Shen, R. Penciuc, M. Kafesaki, C. M. Soukoulis, K. Hingerl, M. Muehlberger & R. Schoeftner: Single and multilayer metamaterials fabricated by nanoimprint lithography, *Nanotechnology* **22**, 325301 (2011)
- [142] F. Xie, A. Centeno, M. R. Ryan, D. J. Riley & N. M. Alford: Au nanostructures by colloidal lithography: from quenching to extensive fluorescence enhancement, *J. Mater. Chem. B* **1**, p. 536 (2012)
- [143] C. L. Haynes & R. P. V. Duyne: A Versatile Nanofabrication Tool for Studies of Size-Dependent Nanoparticle Optics, *J. Phys. Chem. B* **105**, p. 5599-5611 (2001)
- [144] X. Liu, B. Choi, N. Gozubenli & P. Jiang: Periodic arrays of metal nanorings and nanocrescents fabricated by a scalable colloidal templating approach, *J. Colloid Interface Sci.* **409**, p. 52-58 (2013)
- [145] C.-M. Hsu, S. T. Connor, M. X. Tang & Y. Cui: Wafer-scale silicon nanopillars and nanocones by Langmuir-Blodgett assembly and etching, *Appl. Phys. Lett.* **93**, 133109 (2008)
- [146] X. A. Zhang, J. Elek & C.-H. Chang: Three-Dimensional Nanolithography Using Light Scattering from Colloidal Particles, *ACS Nano* **7**, p. 6212-6218 (2013)
- [147] P. Bharadwaj, B. Deutsch & L. Novotny: Optical Antennas, *Adv. Opt. Photon* **1**, p. 438 (2009)
- [148] D.A. Jennings, F.R. Petersen & K.M. Evenson: Extension of absolute frequency measurements to 148 THz: frequencies of 2.0- and 3.5 μm Xe laser, *Appl. Phys. Lett.* **26**, p. 510-511 (1975)
- [149] P. Periasamy, J.J. Berry, A.A. Dameron, J.D. Bergeson, D.S. Ginley, R.P. O'Hayre & P.A. Parilla: Fabrication and Characterisation of MIM Diodes Based on Nb/Nb₂O₅ Via a Rapid Screening Technique, *Adv. Mater.* **23**, p. 3080-3085 (2011)
- [150] J.R. Tucker & M.J. Feldman: Quantum detection at mm wavelengths, *Rev. Mod. Phys.* **57**(4), p. 1055-1114 (1985)
- [151] R.T. Tung: Recent advances in Schottky barrier concepts, *Materials Science and Engineering R* **35**, p. 1-138 (2001)
- [152] R.F. Pierret, *Semiconductor Device Fundamentals*, Addison-Wesley Publishing Company, Inc. USA, 1996

- [153] D.K. Schroder, *Semiconductor Material and Device Characterization, Third Edition*, John Wiley & Sons, Inc., 2006
- [154] S.M. Sze, *Physics of Semiconductor Devices, Third Edition*, John Wiley & Sons, Inc., 2007
- [155] P.M. Gammon, E. Donchev, A. Pérez-Tomás, V.A. Shah, J.S. Pang, P.K. Petrov, M.R. Jennings, C.A. Fisher, P.A. Mawby, D.R. Leadley & N.McN. Alford: A study of temperature-related non-linearity at the metal-silicon interface, *J. Appl. Phys.* **112**, 114513 (2012)
- [156] F. Roccaforte, F. La Via, V. Raineri, R. Pierobon, and E. Zanoni: Extracting the Richardson constant: IrO_x/n-ZnO Schottky diodes, *J. Appl. Phys.* **93**, 9137 (2003).
- [157] P. M. Gammon, A. Pérez-Tomás, V. A. Shah, G. J. Roberts, M. R. Jennings, J. A. Covington, and P. A. Mawby: Analysis of inhomogeneous Ge/SiC heterojunction diodes, *J. Appl. Phys.* **106**, 093708 (2009)
- [158] P. M. Gammon, A. Pérez-Tomás, M. R. Jennings, V. A. Shah, S. A. Boden, M. C. Davis, S. E. Burrows, N. R. Wilson, G. J. Roberts, J. A. Covington & P. A. Mowby: Interface characteristics of $n - n$ and $p - n$ Ge/SiC heterojunction diodes formed by molecular beam epitaxy deposition, *J. Appl. Phys.* **107**, 124512 (2010)
- [159] P. M. Gammon, A. Pérez-Tomás, V. A. Shah, O. Vavassour, E. Donchev, J. S. Pang, M. Myronov, C. A. Fisher, M. R. Jennings, D. R. Leadley & P. A. Mawby: Modelling the inhomogeneous SiC Schottky interface, *J. Appl. Phys.* **114**, 223704 (2013)
- [160] R.T. Tung: Electron transport at metal-semiconductor interfaces: General theory, *Phys. Rev. B* **45**, p. 13509-13523 (1992)
- [161] K.M. Strohm, J. Buechler & E. Kasper: SIMMWIC Rectennas on High-Resistivity Silicon and CMOS Compatibility, *IEEE Trans. Microwave Theory Tech.* **46**(5), p. 669-676 (1998)
- [162] S. Sankaran & K.K. O: Schottky diode with cutoff frequency of 400 GHz fabricated in 0.18 μ m CMOS, *Electronic Letters* **41**(8), p. 506-508 (2005)
- [163] F. Sizov & A. Rogalski: THz detectors, *Quantum Electronics* **34**, p. 278-347 (2010)
- [164] A. Giugni, B. Torre, A. Toma, M. Francardi, M. Malerba, A. Alabastri, R. Proietti Zaccaria, M. I. Stockman & E. Di Fabrizio: Hot-electron nanoscopy using adiabatic compression of surface plasmons, *Nature Nanotechnology* **8**, p. 845-852 (2013)
- [165] B. Eliasson, *Metal-Insulator-Metal Diodes for Solar Energy Conversion*, PhD Thesis at University of Colorado, Boulder, USA, 2001
- [166] T.E. Sullivan, Y. Kuk & P.H. Cutler: Proposed Planar Scanning Tunneling Microscope Diode: Application as an Infrared and Optical Detector, *IEEE Trans. Elec. Devices* **36**(11), p. 2659-2664 (1989)
- [167] R.H. Fowler & L. Nordheim: Electron Emission in Intense Electric Fields, *Proc. R. Soc. Lond. A* **119**, p. 173-181 (1928)
- [168] S. Grover & G. Moddel: Applicability of Metal/Insulator/Metal (MIM) Diodes to Solar Rectennas, *IEEE Journal of Photovoltaics* **1**(1), p. 78-83 (2011)
- [169] S. Grover, S. Joshi & G. Moddel: Quantum theory of operation for rectenna solar cells, *J. Phys. D: Appl. Phys.* **46**, 135106 (2013)
- [170] J. Kadlec & K.H. Gundlach: Dependence of the barrier height on insulator thickness in Al-(Al-Oxide)-Al Sandwiches, *Solid State Communications* **16**, p. 621-623 (1975)
- [171] K. Gloos, P.J. Koppinen & J.P. Pekola: Properties of native ultrathin aluminium oxide tunnel barriers, *J. Phys.: Condens. Matter* **15**, p. 1733-1746 (2003)
- [172] T.K. Gustafson, R.V. Schmidt & J.R. Perucca: Optical detection in thin-film metal-oxide-metal diodes, *Appl. Phys. Lett.* **24**(12), p. 620-622 (1974)
- [173] B. Tiwari, J.A. Bean, G. Szakmány, G.H. Bernstein, P. Fay & W. Porod: Controlled etching and regrowth of tunnel oxide for antenna-coupled metal-oxide-metal diodes, *J. Vac. Sci. Technol. B* **27**(5), p. 2153-2160 (2009)
- [174] M. Heiblum, S. Wang, J.R. Whinnery & T.K. Gustafson: Characteristics of Integrated MOM Junctions at dc and at Optical Frequencies, *IEEE J. Quantum Electronics* **QE-14**(3), p. 159-169 (1978)
- [175] A.B. Hoofring, V.J. Kapoor & W. Krawczonek: Submicron nickeloxidegolf tunnel diode detectors for rectennas, *J. Appl. Phys.* **66**(1), p. 430-437 (1989)
- [176] I. Wilke, Y. Oppliger, W. Herrmann & F.K. Kneubühl: Nanometer Thin-Film Ni-NiO-Ni Diodes for 30 THz Radiation, *Appl. Phys. A* **58**, p. 329-341 (1994)
- [177] M.R. Abdel-Rahman, F.J. González & G.D. Boreman: Antenna-coupled metal-oxide-metal diodes for dual-band detection at 92.5 GHz and 28 THz, *Electronic Letters* **40**(2), (2004)
- [178] P.C.D. Hobbs, R.B. Laibowitz & F.R. Libsch: Ni-NiO-Ni tunnel junction for terahertz and infrared detection, *Applied Optics* **44**(32), p. 6813-6822 (2005)
- [179] S. Krishnan, E. Stefanakos & S. Bhansali: Effects of dielectric thickness and contact area on current-voltage characteristics of thin film metal-insulator-metal diodes, *Thin Solid Films* **516**, p. 2244-2250 (2008)
- [180] K. Choi, F. Yesilkoy, G. Ryu, S.H. Cho, N. Goldman, M. Dagenais & M. Peckerar: A Focused Asymmetric Metal-Insulator-Metal Tunneling Diode: Fabrication, DC Characteristics and RF Rectification Analysis, *IEEE Trans. Electron Devices* **58**(10), p. 3519-3528 (2010)
- [181] P. Esfandiari, G. Bernstein, P. Fay, W. Porod, B. Rakos, A. Zarandy, B. Berland, L. Boloni, G. Boreman, B. Lail, B. Monacelli & A. Weeks: Tunable antenna-coupled metaloxidemetal (MOM) uncooled IR detector (Invited Paper), *Proc. SPIE* **5783**, p. 470482 (2005)
- [182] E.W. Cowell III, N. Alimardani, C.C. Knutson, J.F. Conley Jr., D.A. Keszler, B.J. Gibbons & J.F. Wager: Advancing MIM Electronics: Amorphous Metal Electrodes, *Adv. Mater.* **23**, p. 74-78 (2011)
- [183] N. Alimardani, E.W. Cowell III, J.F. Conley Jr., D.R. Evans, M. Chin, S.J. Kilpatrick & M. Dubey: Impact of electrode roughness on metal-insulator-metal tunnel diodes with atomic layer deposited Al₂O₃ tunnel barriers, *J. Vac. Sci. Tech. A* **30**(1), 01A113 (2012)
- [184] P. Periasamy, R.P. O'Hayre, J.J. Berry, P.A. Parilla, D.S. Ginley & C.E. Packard: A Novel Way to Characterize Metal-Insulator-Metal Devices Via Nanoindentation, *PVSC* **37**, (2011)
- [185] P. Periasamy, H.L. Guthrey, A.L. Abdulagatov, P.F. Ndione, J.J. Berry, D.S. Ginley, S.M. George,

- P.A. Parilla & R.P. O'Hayre: Metal-Insulator-Metal Diodes: Role of the Insulator Layer on the Rectification Performance, *Adv. Mater.* **25**, p. 1301-1308 (2013)
- [186] P. Periasamy, M.S. Bradley, P.A. Parilla, J.J. Berry, D.S. Ginley, R.P. O'Hayre & C.E. Packard: Electromechanical tuning of nanoscale MIM diodes by nanoindentation, *J. Mater. Res.* **28**(14), p. 1912-1919 (2013)
- [187] P. Periasamy, J.D. Bergeson, P.A. Parilla, D.S. Ginley & R.P. O'Hayre: Metal-insulator-metal point-contact diodes as a rectifier for rectenna, *PVSC* **25**, p. 2943-2945 (2010)
- [188] M.L. Chin, P. Periasamy, T.P. O'Regan, M. Amani, C. Tan, R.P. O'Hayre, J.J. Berry, R.M. Osgood, P.A. Parilla, D.S. Ginley & M. Dubey: Planar metal-insulator-metal diodes based on the Nb/Nb₂O₅/X material system, *J. Vac. Sci. Technol. B* **31**(5), 051204 (2013)
- [189] N. Alimardani, J.M. McGlone, J.F. Wager & J.F. Conley Jr: Conduction processes in metal-insulator-metal diodes with Ta₂O₅ and Nb₂O₅ insulators deposited by atomic layer deposition, *J. Vac. Sci. Tech. A* **32**(1), 01A122 (2014)
- [190] E.N. Grossman, T.E. Harvey & C.D. Reintsema: Controlled barrier modification in Nb/NbO_x/Ag metal insulator metal tunnel diodes, *J. Appl. Phys.* **91**(12), p. 10134-10139 (2002)
- [191] J.G. Simmons: Electric Tunnel Effect between Dissimilar Electrodes Separated by a Thin Insulating Film, *J. Appl. Phys.* **34**, p. 2581-2590 (1963)
- [192] I.E. Hashem, N.H. Rafat & E.A. Soliman: Theoretical Study of Metal-Insulator-Metal Tunneling Diode Figures of Merit, *IEEE J. Quantum Electronics* **49**(1), p. 72-79 (2013)
- [193] K. Choi, F. Yesilkoy, A. Chryssis, M. Dagenais & M. Peckerar: New Process Development for Planar-Type CIC Tunneling Diodes, *IEEE Electron Device Letters* **31**(8), p. 809-811 (2010)
- [194] E.W. Cowell III, S.W. Muir, D.A. Keszler & J.F. Wager: Barrier height estimation of asymmetric metal-insulator-metal tunneling diodes, *J. Appl. Phys.* **114**, 213703 (2013)
- [195] S. R. C. McMitchell, Y. Y. Tse, H. Bouyanff, T. J. Jackson, I. P. Jones & M.J. Lancaster: Two-dimensional growth of SrTiO₃ thin films on (001) MgO substrates using pulsed laser deposition and reflection high energy electron diffraction, *Appl. Phys. Lett.* **95**, 174102 (2009)
- [196] R. G. Palgrave, P. Borisov, M. S. Dyer, S. R. C. McMitchell, G. R. Darling, J. B. Claridge, M. Batuk, H. Tan, H. Tian, J. Verbeeck, J. Handermann & M. J. Rosseinsky: Artificial Construction of the Layered Ruddlesden-Popper Manganite La₂Sr₂Mn₃O₁₀ by Reflection High Energy Electron Diffraction Monitored Pulsed Laser Deposition, *J. Amer. Chem. Soc.* **134**, p. 7700-7714 (2012)
- [197] R. Gupta & B.G. Willis: Nanometer spaced electrodes using selective area atomic layer deposition, *Applied Physics Letters* **90**, 253102 (2007)
- [198] M. Bareib, F. Ante, D. Kälblein, G. Jegert, C. Jirauschek, G. Scarpa, B. Fabel, E.M. Nelson, G. Timp, U. Zschieschang, H. Klauk, W. Porod & P. Lugli: High-Yield Printing of Metal-Insulator-Metal Nanodiodes, *ACS Nano* **6**(2), p. 2853-2859 (2012)
- [199] G. Moddel & B.J. Eliasson: High speed electron tunneling device and applications, US Patent No. 6756649B2, 2004
- [200] S. Grover & G. Moddel: Engineering the current-voltage characteristics of metal-insulator-metal diodes using double-insulator barriers, *Solid-State Electronics* **67**, p. 94-99 (2012)
- [201] M. Di Ventura, G. Papp, C. Coluzza, A. Baldereschi & P.A. Schulz: Indented barrier resonant tunneling rectifiers, *J. Appl. Phys.* **80**, p. 4174-4176 (1996)
- [202] B.J. Eliasson & G. Moddel: Metal-oxide Electron Tunneling Device for Solar Energy Conversion, US Patent 6534784B2, 2003
- [203] G. Moddel & B.J. Eliasson: High Speed Electron Tunneling Device and Applications, US Patent 6756649B2, 2004
- [204] B. Hegyi, A. Csurgay & W. Porod: Investigation of the nonlinearity properties of the DC I-V characteristics of metal-insulator-metal (MIM) tunnel diodes with double-layer insulators, *J. Comput. Electron.* **6**, p. 159-162 (2007)
- [205] P. Maraghechi, A. Foroughi-Abari, K. Cadien & A.Y. Elezzabi: Enhanced rectifying response from metal-insulator-insulator-metal junctions, *Appl. Phys. Lett.* **99**, 253503 (2011)
- [206] N. Alimardani, E.W. Cowell, J.F. Wager & J.F. Conley, Jr.: Fabrication and Investigation of Metal-Insulator-Insulator-Metal (MIIM) Tunnel Diodes using Atomic Layer Deposition, *221st ECS Meeting*, (2012)
- [207] N. Alimardani: *Investigation of Metal-Insulator-Metal (MIM) and Nanolaminate Barrier MIIM Tunnel Devices Fabricated via Atomic Layer Deposition*, PhD Thesis at Oregon State University, USA, 2013
- [208] N. Alimardani & J.F. Conley Jr.: Step tunneling enhanced asymmetry in asymmetric electrode metal-insulator-insulator-metal tunnel diodes, *Appl. Phys. Lett.* **102**, 143501 (2013)
- [209] D.C. Sekar, T. Kumar, P. Rabkin & X.C. Costa: MIIM Diode Having Lanthanum Oxide, US Patent 2013/0181181, 2013
- [210] G. Moddel: Geometric Diode, Applications and Method, US Patent 20110017284A1, 2011
- [211] Z. Zhu, S. Grover, K. Krueger & G. Moddel: Optical rectenna solar cells using graphene geometric diodes, *PVSC* **37**, p. 2120-2122 (2011)
- [212] S. Joshi, Z. Zhu, S. Grover & G. Moddel: Infrared optical response of geometric diode rectenna solar cells, *PVSC* **38**, p. 2976-2978 (2012)
- [213] G. Moddel, Z. Zhu, S. Grover & S. Joshi: Ultrahigh speed graphene diode with reversible polarity, *Solid State Communications* **152**, p. 1842-1845 (2012)
- [214] Z. Zhu, S. Joshi, S. Grover & G. Moddel: Graphene geometric diodes for terahertz rectennas, *J. Phys. D: Appl. Phys.* **46**, 185101 (2013)
- [215] S. Grover, *Diodes for optical rectennas*, PhD Thesis at University of Colorado, Boulder, USA, 2011
- [216] N.M. Ashcroft & N.D. Mermin, *Solid state physics*, Orlando: Harcourt College Publishers, 1976
- [217] A.H. Castro Neto, F. Guinea, N.M.R. Peres, K.S. Novoselov & A.K. Geim: The electronic properties of graphene, *Rev. Mod. Phys.* **81**, p. 109-162 (2009)
- [218] M. Fukuda, T. Aihara, K. Yamaguchi, Y.Y. Ling, K. Miyaji & M. Tohyama: Light detection enhanced by surface plasmon resonance in metal film, *Applied Physics Letters* **96**, 153107 (2010)

- [219] T. Ishi, J. Fujikata, K. Makita, T. Baba, K. Ohashi: Si Nano-Photodiode with a Surface Plasmon Antenna, *Jap. J. Appl. Phys.* **44**(2), p. L364-L366 (2005)
- [220] H. Satoh & H. Inokawa: Surface Plasmon Antenna with Gold Line and Space Grating for Enhanced Visible Light Detection by a Silicon-on-Insulator Metal-Oxide-Semiconductor Photodiode, *IEEE Trans. Nanotech.* **11**(2), p. 346-351 (2012)
- [221] M. Bareib, B.N. Tiwari, A. Hochmeister, G. Jegert, U. Zschieschang, H. Klauk, B. Fabel, G. Scarpa, G. Koblmüller, G.H. Bernstein, W. Porod & P. Lugli: Nano Antenna Array for Terahertz Detection, *IEEE Trans. Microwave Theory Trans.* **59**(10), p. 2751-2757 (2011)
- [222] I. Codreanu, F.J. Gonzalez & G.D. Boreman: Detection mechanisms in microstrip dipole antenna-coupled infrared detectors, *Infrared Physics & Technology* **44**, p. 155-163 (2003)
- [223] I. Enderra, R. Gonzalo, B. Martinez, B.E.J. Alderman, P.G. Huggard, A. Murk, L. Marchand & P. de Maagt: Design and Test of a 0.5 THz Dipole Antenna With Integrated Schottky Diode Detector on a High Dielectric Constant Ceramic Electromagnetic Bandgap Substrate, *IEEE Trans. Terahertz Sci. Tech.* **3**(3), p. 584-593 (2013)
- [224] C. Clavero: Plasmon-induced hot-electron generation at nanoparticle/metal-oxide interfaces for photovoltaic and photocatalytic devices, *Nature Photonics* **8**, p. 95-103 (2014)
- [225] The World Bank, (2013): Energy - The Facts, Retrieved from: <http://go.worldbank.org/6ITD8WA1A0>
- [226] Fraunhofer ISE (Press Release 23 Sep. 2013): World Record Solar Cell with 44.7% Efficiency, Retrieved from: <http://www.ise.fraunhofer.de/en/press-and-media/press-releases/presseinformationen-2013/world-record-solar-cell-with-44.7-efficiency>